Politecnico di Torino

Politecnico di Torino

Master's Degree in Physics of Complex Systems

Academic Year 2024/2025

Graduation Session: March 2025

Persistent Exclusion Process: comparative study of mean-field methods and possible generalizations of the model

Supervisors:	**Candidate:**
Prof. Pelizzola Alessandro	Maglione Mauro
	S305412
Dr. Pretti Marco	

Contents

1 Introduction

Biology has been a source of inspiration for non-equilibrium statistical physics, providing many systems in which single agents are able to convert an available source of energy into mechanical work. Birds, ants, bacteria, and cell organelles are all examples of agents that are able to perform complex behaviors in large groups, managing it without the need for a top-down organization to command them. Our interest as complex systems physicists is to develop simplified descriptions of these systems where a set of minimal ingredients is able to reproduce those non-trivial behaviors.
One of the most common simplifications involves discretizing space into a lattice, choosing the simplest topology that captures the physics of the problem under study. The diffusion of this approach has certainly been contributed to by one of the most studied models of non-equilibrium physics, the Totally Asymmetric Simple Exclusion Process (TASEP), which will be referred to later in the thesis. It was first introduced for studying the motion of ribosomes during the translation of mRNA [MGP68], and the discretization had the physical justification that ribosomes move during translation by jumping from one codon to the next. Therefore, they must move in line because the process is optimized for having the highest number of ribosomes passing through and translating the same sequence. The TASEP has later become a cornerstone model for non-equilibrium phase transitions [Kru91] and has been exactly solved. A review on this model that emphasizes its importance as a paradigmatic model for non-equilibrium statistical physics is [CMZ11].
The biological inspiration on which the thesis is founded comes instead from bacterial motion: individual cells like *E. coli* move in a medium via a run-and-tumble dynamics, which is the alternation of straight paths at constant speed and chaotic rotational motion [Ber04]. The fascination with this type of system is part of the larger field of research into active matter, due to the variety of behaviors that emerge when they move collectively: flocking, hydrodynamic interactions, trapping, and phase separation. Dissertations on the physical phenomenologies of run-and-tumble bacteria can be found in the review [EWG15] and in [Cat12].
The lattice model at the center of this thesis was introduced in [Tho+11] to study how flocking and domain formation emerge when density-affected velocity is added to self-propulsion and stochastic reorientation events. The latter fact was demonstrated within the field-theoretic framework [TC08], but a microscopic model was needed to confirm the result. The discretization of space was thus introduced to define, study, and simulate a system where the velocity depends on the local density of particles.
Here, we will consider hard-core run-and-tumble particles, so hopping is not allowed into an occupied site, as it was considered in [SG14] to study the distribution of waiting times in bacterial biofilms, which allows a cell that has been standing still for long enough to differentiate its gene expression. The bacterial motion model we consider has not become as popular as the TASEP, and therefore the need to name it univocally has not yet arisen. Here, to emphasize the connection with the TASEP, we will call it the Persistent Exclusion Process (PEP), because the motion of a particle persists in the same direction between tumbles, and the hard-core interaction is the same excluded volume constraint of the TASEP.
The same model was also proposed for describing counterflowing cargo transportation on microtubules inside eukaryotic cells [MSR11], with particles that can be injected or extracted at the boundaries, whereas the other studies always considered reflecting or periodic boundary conditions. The PEP on a one-dimensional lattice has not proven capable of undergoing phase separation at stationarity, as opposed to its counterparts which allow more than one particle per site. Nevertheless, we found it interesting to treat the model as a variation of the TASEP. With this perspective, we decided to test the pair approximation on the PEP, because it has been successful on other TASEP variants, and we compared the results against other methods used to study the PEP. These were taken from [DCR20], a study that was able to obtain insightful results on the PEP by switching the focus from particles to gaps of empty sites. They also demonstrated that hydrodynamic descriptions of the PEP cannot be defined as simply as for other models, since in this system, the Einstein relation between hydrodynamic quantities does not hold.
In the second part of the thesis, we introduce a more general model that includes both the PEP and the TASEP as limiting cases and explore through simulations how it behaves when coupled

to infinite particle reservoirs at the boundaries. All the simulations performed where done using a kinetic Monte Carlo algorithm, which we describe in some detail in appendix A.

2 Persistent Exclusion Process

In this section we will discuss the persistent exclusion process(PEP), a model for active matter inspired by the motion of bacteria moving in thin biofilms. Bacteria that move using flagella often travel along trajectories composed of linear sections at constant speed, interrupted by quick tumble events where they perform a chaotic rotational motion that makes them change the pointing direction, that happens at time intervals that are Poisson distributed [Ber04]. When many bacteria form a crowd, their ability to move is affected.
The present model for their collective motion is defined on a lattice where each site can be occupied by at most one particle, so they are subject to an exclusion interaction that prevents them from moving if they have another particle in front (we are enforcing crowding in the most strict way).
A configuration of the system is determined if one knows the particles positions and their internal degrees of freedom deciding the direction in which they are moving at a given time. The system evolves in continuous time through two stochastic processes: the run process where a particle makes one step with rate λ if the lattice site in which it points is empty; the tumble process in which the internal degree of freedom changes randomly to a new direction with rate η. The inverse of the jump rate λ is taken as the time unit, and in general all quantities will be considered adimensional.
We are assuming that every single process, with its rate, is associated to a poissonian clock, so that the model follows a random sequential update.
The model particles tend to form clusters. Particles inside a cluster are stuck because the presence of other particles prevents them from hopping, conversely particles at the cluster ends can leave if they tumble in a direction which is clear. The cluster grows by absorbing particles at its ends and shrinks when a particle evaporates by doing a tumble, so clusters are not change their position while their borders move stochastically. Clusters can always form because of the exclusion interaction the smaller η, the longer they will last because evaporation events happen less frequently.
If the tumble happens quickly ($\eta \gg \lambda$), so that a particle changes direction many times before hopping to a new site, then the particle effectively chooses randomly the direction of each step it takes and the model reduces to the Symmetric Simple Exclusion Process (SSEP) [1], where particles simply behave as random walkers with excluded volume. In the opposite limit $\eta = 0$, the Markov chain loses the ergodic property, with different sets of configuration that can be reached for a given starting configuration, because that fixes the directions of the particles. This singular limit will always be ignored.
The system reaches a steady state that does not satisfy detailed balance, so we say that the model is out of equilibrium. This is due to the persistence in the trajectory of each particle. In fact if we consider a system configuration $\mathcal{C}$ with a particle that is moving, it will evolve in the configuration $\mathcal{C}'$ where the particle has moved to the site ahead with rate 1, whereas there is no single transition that can make $\mathcal{C}'$ into $\mathcal{C}$. Since particles can evaporate from clusters the probability $P(\mathcal{C})$ that the system is in a configuration where a particle can move is always different from 0 and detailed balance cannot be satisfied:

$$\begin{cases} W_{\mathcal{C}\mathcal{C}'} P(\mathcal{C}) = W_{\mathcal{C}'\mathcal{C}} P(\mathcal{C}') \\ P(\mathcal{C}) \neq 0 \end{cases} \tag{1}$$

where $W_{\mathcal{C}\mathcal{C}'}$ $W_{\mathcal{C}'\mathcal{C}}$ indicate the rate of transition from configuration $\mathcal{C}$ to $\mathcal{C}'$, which is 1 in the case we considered, and from configuration $\mathcal{C}'$ to $\mathcal{C}$, which is 0 instead.
On a 1D lattice, the situation that will be considered all the time, the internal degree of freedom of a particle can assume only two values $\{-1, +1\}$, indicating the direction in which the lattice is traversed, so that a state of the system can be represented as a collection of variables that indicate the occupation of each site: $n_i \in \{-1, 0, +1\}$, where i assumes values from 1 to L indicating the position on the lattice and an empty site is indicated by a 0.

[1] For references on the SSEP see [Sch01] or [KRB10]

Refer to [SG14] for a discussion of the collective behavior of RTPs subject to excluded volume interaction, focused on the scalings of cluster size and particle stopping time, both in 1D and 2D. These results are expanded in [CMT23], where the effect of the finiteness of the system on the maximum and typical cluster sizes of the system are discussed[2].
The article [DCR20] develops approximated descriptions for high and low tumble regimes that are used to calculate hydrodynamic quantities for the system at stationarity. It is particularly interesting because it switches the description of the system, from the dynamics of particles moving on a lattice to the dynamics of gaps that exchange "masses" depending on the orientation of the neighboring particles. It enables to do approximate calculations with pretty good results. In section 2.1, we will review and expand the results that we need in the discussion of the thesis. In subsequent sections we will use the pair approximation on the PEP and then compare the predictions with the approximations on the mass model. To do so, attention will be paid to the gap distributions and two quantities, namely the average size of particle clusters l_c, a very important quantity for the PEP, and the particle current as a function of the particle density $J(\rho)$, which is important for TASEP-like models where this relation is called the fundamental diagram. Both quantities will depend on the tumbling rate η.
Since at stationarity there is the same average number of particles moving rightward and particles moving leftward, it is straightforward to say that J will be zero, so the actual quantity considered will be the current of particles moving rightward J_+, which has the same magnitude and opposite sign of the current of particles moving leftward J_-.

2.1 Mass Model

We present here the approximated methods used to describe the PEP in the paper [DCR20]. These are based on an alternative description of the PEP where the gaps between particles become the variables describing the state of the system. As it was done in the paper, we will refer to this description as a mass transport model. After the PEP has been mapped, it will be possible to apply the MF approximation, that neglects correlations between different gaps, to obtain approximated results for the stationary mass distribution. The MF is effective only in regimes where the tumble frequency is high (comparable with the rate of motion of particles $\eta \sim \lambda$), so to complete the description a method based on coalescence and fragmentation of masses is used to describe what happens when $\eta \ll \lambda$.
Consider a configuration $\{n_i\}_{i=1}^{L}$ with $N = \sum_{i=1}^{L} |n_i|$ particles that occupy L sites on a ring. Since the particles cannot overtake one another, their order remains fixed and the gaps between particles can be mapped into N masses $\{m_k\}_{k=1}^{N}$, so that each m_k represents the number of empty sites between the k-th and the (k+1)-th particle. If i_k is the position of the k-th particle on the lattice then

$$m_k = i_{k+1} - i_k - 1 \tag{2}$$

where, in order to account for the PBCs, it is sufficient to consider modular arithmetic with modulus L. It is easy to see that the total mass of the system is $\sum_{k=1}^{N} m_k = L - N$, so that the density of the masses in the system can be defined and related to the total density of particles $\rho = \frac{N}{L}$ in the original system

$$\rho_{\text{mass}} = \frac{L-N}{N} = \frac{1}{\rho} - 1 \tag{3}$$

since in this picture masses live on a lattice with N sites. When a particle moves, a unit of mass gets transferred from the mass in front of the particle to the mass behind it. So the mass flow is in the opposite direction w.r.t. the direction the particle is pointing, this is why we encode the particle's directions into spin variables defined as

$$s_{k-\frac{1}{2}} = -n_{i_k} \tag{4}$$

[2]In the model considered in [CMT23] particles can tumble only when they are next to another particle, nonetheless the behavior of the system becomes the same of the PEP when η is small because particles are anyway in clusters most of the time.

where the use of half-integer position indices highlights the fact that the spin determines the direction of the mass flow between two adjacent mass sites. Now it is possible to translate the probability of having at time t a certain configuration in the PEP in the new representation

$$P\left(\{n_i^t\}_{i=1}^L\right) \Leftrightarrow P\left(\{m_k^t\}_{k=1}^N, \left\{s_{k+\frac{1}{2}}^t\right\}_{k=1}^N\right) \tag{5}$$

where t denotes the continuous time variable. From this change of description will come all the following reasoning.

2.1.1 Mean-Field

We derive the steady-state mass distribution within the MF approximation. This method is expected to give better predictions with respect to the MF done over sites because it is better describing the behavior of the gaps between particles, sometimes this is sufficient to get exact results if the correlations within a gap are the only thing that matters in a system [SS97]. The probability of finding the system in a certain configuration of masses $\{m_k\}$ and spins $\{s_{k+\frac{1}{2}}\}$ can always be expressed using the conditional probability:

$$P\left(\{m_k^t\}, \{s_{k+\frac{1}{2}}^t\}\right) = P\left(\{m_k^t\} \middle| \{s_{k+\frac{1}{2}}^t\}\right) P\left(\{s_{k+\frac{1}{2}}^t\}\right) \tag{6}$$

Since each spin flips independently, the probability for the spins at stationarity will be straightforwardly:

$$P\left(\{s_{k+\frac{1}{2}}\}\right) = \prod_k P\left(s_{k+\frac{1}{2}}\right) = \frac{1}{2^N}. \tag{7}$$

In the following it will be assumed that the system is always in a state where the spins have orientations that are randomly distributed with this probability, otherwise we would need to write equations for the dynamical evolution of the spin variables while we are only interested in the behavior of the system at stationarity. The remaining conditional probability is not as simple, this is because the system shows clusters, that become larger for smaller values of η, so the probability of finding two particles next to each other ($m_k = 0$ for some k) will be affected by the piling up of other particles accumulated in the neighboring lattice sites. Nonetheless the following step is to implement a single-site mean-field approximation, where, for each mass, only the neighboring spins get tracked. This allows to rewrite the conditional mass distribution as:

$$P\left(\{m_k\} \mid \{s_{k+\frac{1}{2}}\}\right) \approx \prod_k P\left(m_k \mid s_{k-\frac{1}{2}}, s_{k+\frac{1}{2}}\right)$$

Thus, depending on the four values the spin pair can take, there will be four conditional distributions that we call $P_m^{++}, P_m^{-+}, P_m^{+-}, P_m^{--}$, the superscripts refer to the sign of the spins and express the direction in which the left and the right bonds are making the mass flow. These probability distributions do not depend on the site index since the steady-state is assumed to be translation invariant, as simulations show. For convenience, the following shorthands can be defined:

$$\alpha \equiv P_0^{-+}, \quad \beta \equiv P_0^{++}, \quad \gamma \equiv P_0^{--}, \quad \delta \equiv P_0^{+-} \tag{8}$$

Once the equations that control the distributions at stationarity are solved, they will allow us to write these four quantities in terms of the mass density ρ_{mass} and spin-flip rate η.
The model as it has been defined is characterized by a left-right symmetry that makes $P_m^{++} = P_m^{--}$, because particles hop with rate 1 regardless of their direction. This is a great simplification to the equations because the number of independent probabilities decreases by one, nonetheless here this simplification will be introduced later in order to write the equations in a more general case. In order to do this, the left-right symmetry has to be broken, so it will be assumed that a mass that is transferred to the right, equivalent to a particle moving to the left, does it with rate λ, while the rate of leftward mass transfer is fixed to 1.

First of all the temporal evolution of the probabilities has to be written, then the time derivative may be set at zero because of the steady-state. These equations should describe how the probability of observing a certain configuration at one site of the mass model can be changing in time. Consider, for example, a mass site k that contains m masses and has both neighboring spins pointing rightward $(++)$, this site can be affected by many possible processes, each corresponding to an increase or a decrease of the probability of observing that configuration at a given time. The equation is the following:

$$\begin{aligned}\frac{dP^{++}_{k,m}}{dt} =&\eta\left(P^{+-}_{k,m}+P^{-+}_{k,m}-2P^{++}_{k,m}\right)+\lambda\left(P^{++}_{k,m+1}-(1-\delta_{m,0})P^{++}_{k,m}\right)+\\ &+\lambda\sum_{s=+,-}\sum_{n>0}\frac{1}{2}P^{s+}_{k-1,n}\left((1-\delta_{m,0})P^{++}_{k,m-1}-P^{++}_{k,m}\right)\end{aligned} \tag{9}$$

A short description of the terms on the r.h.s. is:

1. the first term is due to tumbling. Each site can change its state through the flip of one of its neighboring spins
2. the second describes a unit of mass being transferred to site $(k+1)$ since the spin at $(k+\frac{1}{2})$ points rightward. This process cannot happen when the site is empty $(m=0)$
3. the last term describes the transfer of particles from site $(k-1)$ when this site is non empty. Since the process of adding a mass cannot make site k empty, then when $m=0$ only the negative part of this term is present

In order to construct the equations for other configurations of the spins the same three kinds of terms are needed. Assuming translational invariance and using definitions (8) to write the probability that a site is non empty, the MF dynamical equations of the mass model read:

$$\frac{dP^{-+}_{m}}{dt} =\eta\left(P^{++}_{m}+P^{--}_{m}-2P^{-+}_{m}\right)+(1+\lambda)\left(P^{-+}_{m+1}-(1-\delta_{m,0})P^{-+}_{m}\right) \tag{10}$$

$$\begin{aligned}\frac{dP^{++}_{m}}{dt} =&\eta\left(P^{+-}_{m}+P^{-+}_{m}-2P^{++}_{m}\right)+\lambda(P^{++}_{m+1}-(1-\delta_{m,0})P^{++}_{m})+\\ &+\frac{\lambda}{2}(2-\alpha-\beta)\left((1-\delta_{m,0})P^{++}_{m-1}-P^{++}_{m}\right)\end{aligned} \tag{11}$$

$$\begin{aligned}\frac{dP^{--}_{m}}{dt} =&\eta\left(P^{+-}_{m}+P^{-+}_{m}-2P^{--}_{m}\right)+(P^{--}_{m+1}-(1-\delta_{m,0})P^{--}_{m})+\\ &+\frac{1}{2}(2-\alpha-\gamma)\left((1-\delta_{m,0})P^{--}_{m-1}-P^{--}_{m}\right)\end{aligned} \tag{12}$$

$$\begin{aligned}\frac{dP^{+-}_{m}}{dt} =&\eta\left(P^{++}_{m}+P^{--}_{m}-2P^{+-}_{m}\right)+\\ &+\frac{1}{2}\left[(2-\alpha-\gamma)+\lambda(2-\alpha-\beta)\right]\left((1-\delta_{m,0})P^{+-}_{m-1}-P^{+-}_{m}\right)\end{aligned} \tag{13}$$

In the steady state, time derivatives vanish and equations (10-13) become a system of coupled difference equations. The equations at stationarity can serve as recursive relations that allow one to obtain the values of the distributions for $m>0$ knowing $\alpha,\beta,\gamma,\delta$. This justifies the statement that the MF equations are solved once the aforementioned four probabilities are written in terms of the parameters.
To solve the system, the generating function method may be used since stationary probabilities are defines by recursion relations, so we define:

$$\tilde{P}^{ss'}(z)=\sum_{m=0}^{\infty}P^{ss'}_{m}z^{m}$$

Multiplying each of the equations (10-13) by z^m and summing over m, the following linear system can be obtained:

$$\begin{cases} \eta z(\tilde{P}^{--}(z) + \tilde{P}^{++}(z) - 2\tilde{P}^{-+}(z)) = (1+\lambda)(z-1)(\tilde{P}^{-+}(z) - \alpha) \\ \eta z(\tilde{P}^{-+}(z) + \tilde{P}^{+-}(z) - 2\tilde{P}^{++}(z)) = \lambda(z-1)(\tilde{P}^{++}(z) - \beta - \frac{1}{2}z(2-\alpha-\beta)\tilde{P}^{++}(z)) \\ \eta z(\tilde{P}^{-+}(z) + \tilde{P}^{+-}(z) - 2\tilde{P}^{--}(z)) = (z-1)(\tilde{P}^{--}(z) - \gamma - \frac{1}{2}z(2-\alpha-\gamma)\tilde{P}^{--}(z)) \\ \eta(\tilde{P}^{--}(z) + \tilde{P}^{++}(z) - 2\tilde{P}^{+-}(z)) = \frac{1}{2}(1-z)\left(\lambda(2-\alpha-\beta) + (2-\alpha-\gamma)\right)\tilde{P}^{+-}(z) \end{cases} \tag{14}$$

where the following relations have been used:

$$\sum_{m=0}^{\infty} z^m(1-\delta_{m,0})P_{m-1}^{ss'} = z\tilde{P}^{ss'}(z) \qquad \sum_{m=0}^{\infty} z^m P_{m+1}^{ss'} = \frac{\tilde{P}^{ss'}(z) - P_0^{ss'}}{z}$$

Before solving the system for the generating functions, it is convenient to restore the left-right symmetry in order to reduce the number of unknowns and parameters, making the expressions of the solutions more manageable. This is obtained by choosing $\lambda = 1$, which implies that:

$$\tilde{P}^{--}(z) = \tilde{P}^{++}(z) \qquad \gamma = \beta$$

The expressions for the generating functions turn out to be:

$$\tilde{P}^{++}(z) = \frac{2\left[(\alpha+\beta-2)(z-1)+2\eta\right]\left[(\alpha+\beta)\eta z + \beta(z-1)\right]}{h(z)} \tag{15}$$

$$\tilde{P}^{+-}(z) = \frac{4\eta\left[(\alpha+\beta)\eta z + \beta(z-1)\right]}{h(z)} \tag{16}$$

$$\begin{aligned} \tilde{P}^{-+}(z) = \frac{1}{h(z)}\Big\{ & 2\eta(z-1)\left(3\alpha^2 z + \alpha((4\beta-6)z+2) + (\beta-2)\beta z\right) + \\ & + 4\eta^2 z(\alpha+\beta) + \alpha(z-1)^2(\alpha+\beta-2)(z(\alpha+\beta-2)+2)\Big\} \end{aligned} \tag{17}$$

where the denominator of all three expressions is:

$$h(z) = \left[(\alpha+\beta-2)(1+\eta)z + 2 - \alpha - \beta + 2\eta\right]\left[(\alpha+\beta-2)z^2 + (4-\alpha-\beta+4\eta)z - 2\right] \tag{18}$$

By setting $z = 0$ in the expression of $\tilde{P}^{+-}(z)$, one obtains the result:

$$\delta = \frac{2\eta\beta}{2\eta + 2 - \alpha - \beta} \tag{19}$$

The remaining quantities α and β need some additional considerations, if we want to be able to determine their expressions. The first consideration regards how the mass distributions should behave for large m, the second comes from the fact that the number of particles in the system is conserved so there is a constraint due to the mass density ρ_{mass}. The asymptotic behavior of the distribution $P_m^{ss'}$ is determined by the poles of the generating functions, namely, if z^* is the smallest pole then

$$P_m^{ss'} \sim e^{-m/m^*} \quad \text{with} \quad m^* = \frac{1}{\ln z^*}$$

The expression (18) is factorized and its zeros, which are the poles, can easily be obtained:

$$\begin{aligned} z_1 &= \frac{2-\alpha-\beta+2\eta}{(1+\eta)(2-\alpha-\beta)} \\ z_2 &= \frac{\alpha+\beta-4\eta-4+\sqrt{(\alpha+\beta-4\eta)^2+32\eta}}{2(\alpha+\beta-2)} \\ z_3 &= \frac{\alpha+\beta-4\eta-4-\sqrt{(\alpha+\beta-4\eta)^2+32\eta}}{2(\alpha+\beta-2)} \end{aligned}$$

Among these, it can be shown that $z_1, z_2 > 1$ and $z_3 < 1$. From the expression of m^*, it can be seen that poles smaller than unity imply a diverging behavior of the mass distributions, which is not possible because they must remain finite and normalizable, in order to be physically meaningful. In order to prevent the divergence at z_3 one can impose that the numerators of the generating functions (15) vanish exactly at z_3. The result of these requirements is one constraint that is valid for all three expressions:

$$\alpha = \frac{2\beta\sqrt{\beta + 2\eta + \eta^2} - \beta^2}{\beta + 2\eta} \tag{20}$$

Now we consider the number of particles in the system. In particular it is necessary to connect the generating functions to the mass density, which is a conserved quantity. First, one has to define the generating function associated to the probability of finding a generic gap unconditioned on the neighboring spin:

$$P_m = \frac{1}{4}P_m^{-+} + \frac{1}{2}P_m^{++} + \frac{1}{4}P_m^{+-} \tag{21}$$

$$\tilde{P}(z) = \sum_{m=0}^{\infty} z^m P_m = \frac{1}{4}\tilde{P}^{-+}(z) + \frac{1}{2}\tilde{P}^{++}(z) + \frac{1}{4}\tilde{P}^{+-}(z) \tag{22}$$

so that the average gap size, the mass density, can be written as

$$\rho_{\text{mass}} = \sum_{m=0}^{\infty} mP_m = z\frac{\mathrm{d}\tilde{P}(z)}{\mathrm{d}z}\bigg|_{z=1} \tag{23}$$

$$\Rightarrow \qquad 1 - \frac{1}{\rho} = \frac{(\alpha+\beta)(3\alpha+\beta) + 8(2-2\alpha-\beta)}{8\eta(\alpha+\beta)} + \frac{2-\alpha-\beta}{\alpha+\beta} \tag{24}$$

where the relation between ρ and ρ_{mass}, present in equation (3), has been used. Constraints (20) and (24) can be used to obtain α and β as functions of η and ρ, so that all steady state quantities regarding the MF mass model can be determined, further details can be found in [DCR20].
The predictions of the MF mass model match well with Monte Carlo simulations when many tumble happen in the time needed for a particle to collide with another, since the mean distance between particles is ρ^{-1}, this translates to $\eta^{-1} \ll \rho^{-1}$ [DCR20]. Since deviations occur for small η, this indicates that clustering is not captured well enough by the mean-field approximation.

2.1.2 Observables in the Mean-Field Mass Model

The current J_+ is the probability of finding a lattice site occupied by a particle pointing in the positive direction and an empty site in front of it, multiplied by the unitary rate of motion. This has to be translated in terms of the mass model. Here, it is important to note that in order to relate the pair marginals probabilities defined over sites to the probabilities of the mass model, that are instead defined over particles, one has to take into account the conditioning on the probability to find a given lattice site occupied. Since the system is translationally invariant at stationarity, any site i can be picked and the probability that it will be occupied by one of

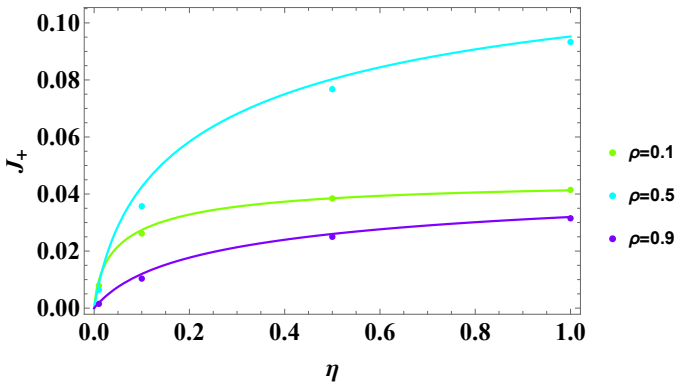

Figure 1: Rightward current J_+ plotted against rate of tumble η. Dots represent simulated values of the current (system size $L = 500$), while the continuous line is the current predicted by the MF mass model

the N particles will be $\frac{N}{L}$, the probability of any orientation is $\frac{1}{2}$. These have to be multiplied to the probability of having a gap of any size in front of it. With all these considerations, we can write the probability that the generic k-th particle is occupying the generic i-th site and the site in front of it is empty:

$$\begin{aligned} J_+ &= \mathbb{P}\left[n_i = 1, n_{i+1} = 0\right] = \mathbb{P}\left[n_i = 1\right]\mathbb{P}\left[n_{i+1} = 0 | n_i = 1\right] = \\ &= \frac{1}{2}\frac{N}{L}\sum_{s=+,-}\mathbb{P}\left[s_{k+\frac{1}{2}} = s\right]\mathbb{P}\left[m_k > 0 | s_{k-\frac{1}{2}} = -1, s_{k+\frac{1}{2}} = s\right] \\ &= \frac{1}{2}\frac{N}{L}\sum_{s=+,-}\frac{1}{2}\sum_{m>0}P_m^{-,s} = \frac{\rho}{4}(2-\alpha-\beta) \end{aligned} \tag{25}$$

Note that this is an exact relation, the approximation lays in the fact that $\alpha(\rho,\eta)$ and $\beta(\rho,\eta)$ assume their MF values.
As it can be seen from figure1, the MF mass model is able to give a pretty good estimate of the values observed in the simulations, which improves as the value of η increases. A plot of the current as function of ρ can be found in figure8 in section 2.3, where the predictions of different methods will be compared.

Now consider the average cluster size l_c. A cluster is a contiguous sequence of lattice sites occupied by a particle, regardless of the orientations. The quantity l_c will be the average of the lengths weighted by the probability of finding the cluster of that length in the system. A possible reasoning to obtain this probability is the following: first define the probability that picking a random site on the lattice, it has on its right an empty site, followed by l occupied sites and another empty site after these

$$P_s(l) = \mathbb{P}\left[n_0 = 0, n_1 \neq 0, ...n_l \neq 0, n_{l+1} = 0\right] \tag{26}$$

then this can be used to evaluate the probability that picking a random site i it belongs to a cluster of size l and the probability that i belongs to a generic cluster

$$\mathbb{P}\left[\text{find a cluster of size } l\right] = P_s(l) \qquad \mathbb{P}\left[\text{find a cluster of any size}\right] = \sum_{h=1}^{\infty}P_s(h) \tag{27}$$

Note that we are also including single particles as clusters of size 1 and so the sum starts from 1. The probability distribution of the cluster sizes $P_c(l)$ will be given by the probability to have found a cluster of a specific size, in any site of the lattice, conditioned on the probability to have found a generic cluster on the lattice. In this way $P_c(l)$ is a probability defined over clusters

$$P_c(l) = \mathbb{P}\left[\text{find a cluster of size } l | \text{find a cluster}\right] = \frac{\mathbb{P}\left[\text{find a cluster of size } l\right]}{\mathbb{P}\left[\text{find a cluster}\right]} = \frac{P_s(l)}{\sum_{h=1}^{\infty}P_s(h)} \tag{28}$$

Using this, the average over the clusters sizes can be performed

$$l_c = \sum_{l=1}^{\infty}lP_c(l) = \frac{\sum_{l=1}^{\infty}lP_s(l)}{\sum_{h=1}^{\infty}P_s(h)} \tag{29}$$

To use this formula we write (26) in the terms of the mass model. As in the case of the current, to pass from a probability defined over sites, to one defined over particles, it is needed to condition on

the probability to find a particle at a site, so we write:

$$\begin{aligned}
P_s(l) =& \mathbb{P}[n_1 \neq 0] \frac{\mathbb{P}\left[n_0 = 0, n_1 \neq 0, ...n_l \neq 0, n_{l+1} = 0\right]}{\mathbb{P}[n_1 \neq 0]} = \\
=& \frac{N}{L} \sum_{\{\sigma_{k-\frac{1}{2}}=+,-\}_{k=0}^{l+1}} \mathbb{P}\left[m_0 > 0, m_1 = 0, ..., m_{l-1} = 0, m_l > 0; s_{-\frac{1}{2}} = \sigma_{-\frac{1}{2}}, ..., s_{l+\frac{1}{2}} = \sigma_{-\frac{1}{2}}\right] \approx \\
\approx& \frac{\rho}{2^{l+2}} \sum_{\{\sigma_{k-\frac{1}{2}}=+,-\}_{k=0}^{l+1}} \sum_{m_0>0} P_{m_0}^{\sigma_{-\frac{1}{2}}\sigma_{\frac{1}{2}}} \prod_{h=1}^{l-1} P_0^{\sigma_{h-\frac{1}{2}}\sigma_{h+\frac{1}{2}}} \sum_{m_l>0} P_{m_l}^{\sigma_{l-\frac{1}{2}}\sigma_{l+\frac{1}{2}}} = \\
=& \frac{\rho}{2^{l+2}} \begin{pmatrix} 2-\alpha-\beta \\ 2-\delta-\beta \end{pmatrix}^T \begin{pmatrix} \beta & \delta \\ \alpha & \beta \end{pmatrix}^{l-1} \begin{pmatrix} 2-\delta-\beta \\ 2-\alpha-\beta \end{pmatrix}
\end{aligned} \tag{30}$$

where the last form uses the matrices to write the expression in a more compact way. By further manipulating the expression it is possible to write the following:

$$\begin{aligned}
P_s(l) = \frac{2^{-l-3}\rho}{\sqrt{\alpha\delta}} \Big\{ & \left(\sqrt{\alpha}+\sqrt{\delta}\right)^2 \left(\sqrt{\alpha\delta}+\beta-2\right)^2 \left(\sqrt{\alpha\delta}+\beta\right)^{l-1} + \\
& - \left(\sqrt{\alpha}-\sqrt{\delta}\right)^2 \left(\sqrt{\alpha\delta}-\beta+2\right)^2 \left(\beta-\sqrt{\alpha\delta}\right)^{l-1} \Big\}
\end{aligned} \tag{31}$$

This probability depends on l through an exponential so expressions (28) and (29) can be evaluated using the geometric series

$$\sum_{l=1}^{\infty} x^l = \frac{x}{1-x} \qquad \sum_{l=1}^{\infty} l x^l = \frac{x}{(1-x)^2} \tag{32}$$

obtaining

$$\sum_{l=1}^{\infty} P_s(l) = \frac{\rho}{4}(4-\alpha-2\beta-\delta) \qquad \sum_{l=1}^{\infty} l P_s(l) = \rho$$

Now we evaluate their ratio, so that the average cluster size reads

$$l_c = \frac{4}{4-\alpha-2\beta-\delta} \tag{33}$$

2.1.3 Coalescence Fragmentation Picture

Now we briefly discuss the coalescence fragmentation model that describes the PEP in the limit $\eta \to 0$: when η is small, there is an evident separation of the time scales, the one related to tumble events η^{-1}, and the one in which particles move between clusters, so that mass transfers occur instantaneously with respect to the first. This translates into the fact that masses move toward mass sites with neighboring spins $+-$, and remain on those sites until one of the neighboring spins flips. This framework has been described in [DCR20] to address the relaxation to the steady state, obtaining scaling forms for the time dependent quantities. We will only talk about the steady state. These kind of models are commonly denoted as reaction-diffusion processes, for an introduction to the topic refer to [KRB10].
Imagine to coarse-grain time and observe the system at time scales of the order of η^{-1}. Let us denote with an A a site with non-zero mass and with $\emptyset$ an empty site. A typical configuration has all sites with spin configuration $+-$ that are either A or $\emptyset$, while all the other sites with different spins are $\emptyset$, other kinds of configurations are transient. When a spin flips on one side of a site of type A then a mass transfer is triggered, targeted toward the nearest site in configuration $+-$ that is in the same direction of the flipped spin, there are three possible outcomes:

- diffusion: the target site is an empty one, then the entire mass gets transferred there, with A and $\emptyset$ simply interchanging positions;

- coalescence: the target site is non-empty, so the mass is added to the target A and the original A has vanished;
- fragmentation: during the transient of the mass transfer a spin flip occurs in one of the sites between the original and the target one, blocking a fraction of the mass that ends up split between the target site and the site where the spin has flipped, so that an additional A gets produced.

Now we use an heuristic argument to evaluate the stationary density of non-empty sites n_c (number of A sites over N) and the typical mass size m^*: in order to be a steady state the total rate at which new sites of type A appear must be equal to the total rate at which they disappear, otherwise the density of clusters would grow or decrease over time. So we need to evaluate the total rate of coalescence r_c and the total rate of fragmentation r_f.
Non-empty sites must have spins in configuration $+-$, so it is impossible to find two sites with A next to each other. In addition we assume that A sites are sparse $n_c \ll 1$, and each site is independently occupied or empty with probability n_c and $1-n_c$ respectively. If the latter was true we could write that the possibility to find two A at a distance n is $n_c^2(1-n_c)^{n-1}$, but we can write an approximate form for small n_c

$$n_c^2(1+\epsilon(n)) \tag{34}$$

where $\epsilon(n)$ is a correction $O(n_c)$.
In order for an A to diffuse into another A site and coalesce after a spin flip, it must happen that all the spins in between the two A sites point in the same direction. One of the spins is already pointing in the needed direction because it belongs to the target A site, so the probability that the spins are in the right direction is $(\frac{1}{2})^{n-2}$. The total probability of finding two A in the right condition times the frequency at which one of the two spins neighboring an A flips gives the total rate of coalescence:

$$r_c = 2\eta \sum_{n\geq 2} 2^{-n+2}\, n_c^2(1+\epsilon(n)) = 4\eta\, n_c^2 + O(\eta\, n_c^3) \tag{35}$$

Let us turn our attention to fragmentation. Consider a site A, with rate η one of its spins can flip, initiating a mass transfer in the spin's new direction. Suppose that the right spin flips, becoming positive, and that the target site is at a distance of $k \geq 1$ sites. Since the target can be either empty or occupied, the probability of it being at a distance k is equal to the probability of having a number $k-1$ of "+" spins consecutively after the one that flipped and the successive being "−". So we have that the rate at which a mass transfer over k sites happens is $\eta\, n_c\, 2^{-k}$. The mass transfer can give place to a fragmentation in two ways:

- the + spin on the left of the original site flips so that part of the original mass is transferred to another target site on the left;
- the transfer gets interrupted on the right by the flip of one of the + spins, so that the transfer to the target site is partial and the rest of the mass stays where the spin has flipped;

if the spin flip during transfer happens on the left of the target site the outcome would be that all the mass is transferred to the site in the left of the target site, resulting in a diffusion at a distance $k-1$, without fragmentation. The event that splits the transfer has to happen during the time of the transfer, so if we assume that this time is roughly $m^* + \delta(k)$, where m^* is the typical mass of an A and $\delta(k)$ is a correction $o(m^*)$, we can say that the rate at which a transfer over k sites leads to a fragmentation is

$$\eta\, k\, (m^* + \delta(k)) \tag{36}$$

If we consider that what we described leads to the same result if the first spin to flip is on the left of the original A site, then the total rate of fragmentation is

$$r_f = 2\sum_{k\geq 1} \eta\, n_c\, 2^{-k}\, \eta\, k\, (m^* + \delta(k)) = 4\,\eta^2\, n_c\, m^* + O(\eta^2\, n_c) \tag{37}$$

By equating the rate of coalescence and fragmentation we get

$$r_c = r_f \qquad \rightarrow \qquad 4\,\eta\,n_c^2 = 4\,\eta^2\,n_c\,m^* \qquad \rightarrow \qquad n_c = \eta\,m^* \tag{38}$$

the latter relation can be used with the constraint $m^*\,n_c = \frac{L-N}{N} = \frac{1}{\rho} - 1$ to obtain

$$n_c^2 = \eta\left(\frac{1-\rho}{\rho}\right) \qquad m^* = \sqrt{\frac{1-\rho}{\rho\,\eta}} \tag{39}$$

These results are consistent with the assumptions we made. The inverse of the density of A sites gives the average distance between non-empty sites which corresponds to the cluster size in the picture of run and tumble particles

$$l_c = \frac{1}{n_c} = \sqrt{\frac{\rho}{(1-\rho)\,\eta}} \tag{40}$$

These results match well with simulations done at $\eta \ll 1$. In section 3 we use this same reasoning to estimate the cluster size for other models. A scaling behavior of this form has been found to be universal throughout many models of active matter [Dol+20]. In [DCR20] the coalescence fragmentation model has been used also to obtain the scalings for the relaxation of the system toward stationarity at small η.

2.2 Pair Approximation

In this section we switch to consider the so-called pair approximation. This method tries to improve the MF by assuming that the probability measure of the configuration over lattice sites factorizes in pair marginals instead of single site marginals. The necessity of using this refinement of the MF for describing the PEP, comes from the fact that this method cannot capture the dependence on η shown by the simulated system, at stationarity. This will be displayed after the definition of some quantities and the description of the equations governing their time evolution.

Using the PA, the problem of describing the system passes from that of solving the time evolution of the probability of a full configuration $P(\{n_i^t\}_{i=1}^L)$, which means characterizing 3^L time dependent quantities, one for each possible configuration, to the problem of characterizing L probability distributions $P(n_i^t, n_{i+1}^t)$, one for each pair of adjacent sites, that can take $3^2 - 1$ independent values. One has to enforce also that single site marginals are consistent between pairs that share a site, giving two additional constraints that lower to $6L$ the number of quantities needed to describe the system in this approximation.
To lighten the notation for the marginal probabilities, that will appear also in other sections, we introduce a way of writing probabilities for configurations of adjacent sites:

$$P_i^t[\nu_1, \nu_2, ..., \nu_{l-1}] = \mathbb{P}[n_i^t = \nu_1, n_{i+1}^t = \nu_2, ..., n_{i+l}^t = \nu_{l-1}] \tag{41}$$

The same notations without the t superscript will be used for time independent quantities at stationarity. The set of marginal probabilities that become our variables in the discussion of the PA can be chosen with some freedom, here we have used

$$\begin{cases} \rho_{+,i}^t = P_i^t[1] \\ \rho_{-,i}^t = P_i^t[-1] \\ \phi_{++,i}^t = P_i^t[1,1] \\ \phi_{--,i}^t = P_i^t[-1,-1] \\ \phi_{+-,i}^t = P_i^t[1,-1] \\ \phi_{-+,i}^t = P_i^t[-1,1] \end{cases} \qquad \text{for } i \in \{1, ..., L\} \tag{42}$$

When $i = L$ the second site is $i + 1 = 1$, for taking into account the PBCs.
Thanks to the simplification from an exponential problem ($\#\,of\ variables \sim 3^L$) to a linear problem

($\#\, of\ variables \sim L$), the implementation of numerical techniques becomes feasible for systems with system sizes $L \sim 100$ sites even for a common PC. So it was possible to numerically integrate the $6L$ equations describing the dynamical evolution of the marginals, for given values of the tumble rate η and system size L, starting from certain initial conditions for the probabilities (that implicitly set the number of particles in the system and consequently ρ) up to some final time T. After the integration we evaluated the stability of the resulting stationary state profiles, in order to verify in a more rigorous way the validity of the integration that, by itself, cannot guarantee that the operation has reached a true stationary configuration.
The dynamical equations for the chosen marginals are obtained by marginalizing the master equation governing the time evolution of $P\left(\{n_i^t\}_{i=1}^L\right)$, the probability that the system is in some configuration at time t. The equations contain three-site marginals that need to be rewritten using the PA

$$P_i^t[\sigma_1,\sigma_2,\sigma_3] \approx \frac{P_i^t[\sigma_1,\sigma_2]P_i^t[\sigma_2,\sigma_3]}{P_i^t[\sigma_2]} \tag{43}$$

In this way a set of differential equations that is closed with respect to the pair and single-site marginals is obtained. The equations read

$$\frac{\mathrm{d}\rho_{+,i}^t}{\mathrm{d}t} = \eta(\rho_{-,i}^t - \rho_{+,i}^t) + \lambda_1(\rho_{+,i-1}^t - \phi_{++,i-1}^t - \phi_{+-,i-1}^t) - \lambda_1(\rho_{+,i}^t - \phi_{++,i}^t - \phi_{+-,i}^t) \tag{44}$$

$$\frac{\mathrm{d}\rho_{-,i}^t}{\mathrm{d}t} = \eta(\rho_{+,i}^t - \rho_{-,i}^t) + \lambda_2(\rho_{-,i-1}^t - \phi_{-+,i-1}^t - \phi_{--,i-1}^t) - \lambda_2(\rho_{-,i}^t - \phi_{-+,i}^t - \phi_{--,i}^t) \tag{45}$$

$$\begin{aligned}\frac{\mathrm{d}\phi_{++,i}^t}{\mathrm{d}t} &= \eta(\phi_{+-,i}^t + \phi_{-+,i}^t - 2\phi_{++,i}^t) + \\ &+ \lambda_1\frac{(\rho_{+,i-1}^t - \phi_{++,i-1}^t - \phi_{+-,i-1}^t)(\rho_{+,i+1}^t - \phi_{++,i}^t - \phi_{-+,i}^t)}{1-\rho_{+,i}^t-\rho_{-,i}^t} + \\ &- \lambda_1\frac{\phi_{++,i}^t(\rho_{+,i+1}^t - \phi_{++,i+1}^t - \phi_{+-,i+1}^t)}{\rho_{+,i+1}^t}\end{aligned} \tag{46}$$

$$\begin{aligned}\frac{\mathrm{d}\phi_{+-,i}^t}{\mathrm{d}t} &= \eta(\phi_{++,i}^t + \phi_{--,i}^t - 2\phi_{+-,i}^t) + \\ &+ \lambda_1\frac{(\rho_{+,i-1}^t - \phi_{++,i-1}^t - \phi_{+-,i-1}^t)(\rho_{-,i+1}^t - \phi_{+-,i}^t - \phi_{--,i}^t)}{1-\rho_{+,i}^t-\rho_{-,i}^t} + \\ &+ \lambda_2\frac{(\rho_{+,i}^t - \phi_{++,i}^t - \phi_{+-,i}^t)(\rho_{-,i+2}^t - \phi_{+-,i+1}^t - \phi_{--,i+1}^t)}{1-\rho_{+,i+1}^t-\rho_{-,i+1}^t}\end{aligned} \tag{47}$$

$$\begin{aligned}\frac{\mathrm{d}\phi_{-+,i}^t}{\mathrm{d}t} &= \eta(\phi_{++,i}^t + \phi_{--,i}^t - 2\phi_{-+,i}^t) + \\ &- \lambda_2\frac{\phi_{-+,i}^t(\rho_{-,i}^t - \phi_{-+,i}^t - \phi_{--,i}^t)}{\rho_{+,i+1}^t} - \lambda_1\frac{\phi_{-+,i}^t(\rho_{+,i+1}^t - \phi_{++,i+1}^t - \phi_{+-,i+1}^t)}{\rho_{+,i+1}^t}\end{aligned} \tag{48}$$

$$\begin{aligned}\frac{\mathrm{d}\phi_{--,i}^t}{\mathrm{d}t} &= \eta(\phi_{+-,i}^t + \phi_{-+,i}^t - 2\phi_{--,i}^t) + \\ &+ \lambda_2\frac{(\rho_{-,i-1}^t - \phi_{-+,i-1}^t - \phi_{--,i-1}^t)(\rho_{-,i+1}^t - \phi_{+-,i}^t - \phi_{--,i}^t)}{1-\rho_{+,i}^t-\rho_{-,i}^t} + \\ &- \lambda_2\frac{(\rho_{-,i}^t - \phi_{-+,i-1}^t - \phi_{--,i-1}^t)\phi_{--,i}^t}{\rho_{-,i}^t}\end{aligned} \tag{49}$$

Before discussing the numerical solutions of these equations let us make some considerations.
The simulations show that the system, at stationarity, reaches a homogeneous state, so it makes sense to search for a solution of equations (44) that is uniform over sites.
By setting time derivatives at zero, and eliminating the dependence on the lattice indices in the equations for $\dot{\rho}_{+,i}^t$ and $\dot{\rho}_{-,i}^t$, it is straightforward to see that the terms associated to particles hopping

cancel out and the equations just impose that, at a given site, the probability of finding a particle pointing rightward or leftward is the same, so that the uniform density profile is the one where

$$\rho_{+.i} = \rho_{-,i} = \frac{1}{2}\rho = \frac{1}{L}\sum_{i=1}^{L}(\rho^0_{+,i} + \rho^0_{-,i}) \qquad \forall i \in \{1, ..., L\} \tag{50}$$

Here we have the opportunity to explain why the simple MF is not enough to describe the PEP. In fact this approximation can only give predictions for the single site marginals, and from the previous result, that is valid also in the case of MF, we see that the homogeneous stationary state would have had no trace of the tumbling dynamics and its consequences. The density ρ is independent of η, consequently any quantity written in MF approximation, using only single site marginals, would have been wrong. Only in the limit $\eta \to \infty$ the MF is a good description as the system becomes a symmetric simple exclusion process, whose stationary probability measure factorizes over sites.

Now we go back to the discussion of the homogeneous solution of (44). To obtain relations for the pair marginals it is sufficient to substitute the values of the single-site marginals (50) in the remaining equations in which time and space invariance has been imposed, so that the equations' variables are $\phi_{++}, \phi_{+-}, \phi_{-+}, \phi_{--}$, without the site and time indices. Homogeneity and the fact that there is the same probability of finding particles independently of their orientation, implies that $\phi_{++} = \phi_{--}$, in this way the net current at stationarity is equal to 0. So in the end a system of equations in three variables is obtained:

$$\begin{cases} \eta(1-\rho)(\phi_{++} - \phi_{+-}) + \left(\frac{\rho}{2} - \phi_{++} - \phi_{+-}\right)^2 = 0 \\ \eta\frac{\rho}{2}(\phi_{++} - \phi_{-+}) - \phi_{-+}\left(\frac{\rho}{2} - \phi_{++} - \phi_{+-}\right) = 0 \\ \eta\frac{\rho}{2}(1-\rho)(\phi_{+-} + \phi_{-+} - 2\phi_{++}) - \phi_{++}(1-\rho)\left(\frac{\rho}{2} - \phi_{++} - \phi_{+-}\right) + \\ \qquad\qquad + \frac{\rho}{2}\left(\frac{\rho}{2} - \phi_{++} - \phi_{+-}\right)\left(\frac{\rho}{2} - \phi_{++} - \phi_{-+}\right) = 0 \end{cases} \tag{51}$$

Unfortunately the non-linear nature of the equations makes it difficult to obtain all solutions in closed form, so we used the Mathematica software to obtain the values of the marginals as a function of the tumble rate η and the density ρ.
One simple solution of the system is the following:

$$\phi_{++} = \phi_{+-} = \phi_{-+} = \frac{\rho}{4} \tag{52}$$

This solution implies the absence of currents $J_\pm = \frac{\rho}{2} - \phi_{++} - \phi_{+-} = 0$ in the system. Unfortunately it does not make sense as a global solution unless the system is completely full, $\rho = 1$, or empty, $\rho = 0$.
Fortunately the other solution actually depends on η, this can be seen in figure 2 where the values of $\phi_{++}, \phi_{+-}, \phi_{-+}$ obtained by numerically solving (51) have been plotted against η, for a fixed density $\rho = 0.5$. These predictions are compared with simulations and results of the other method in the next section, in Fig 7. It can be said that the PA is always worse than the other approximation.

2.2.1 Observables in Pair Approximation

In order to compare the PA with the MF mass model we derive the approximated expressions for our quantities of interest, the current $J_\pm$ and the average cluster size l_c, plus the gap size distribution for a direct comparison of the two approximations:

- The current is the probability to find a particle that can hop in the site in which it is pointing, times the unitary hopping rate, so, considering any site i of the translationally invariant

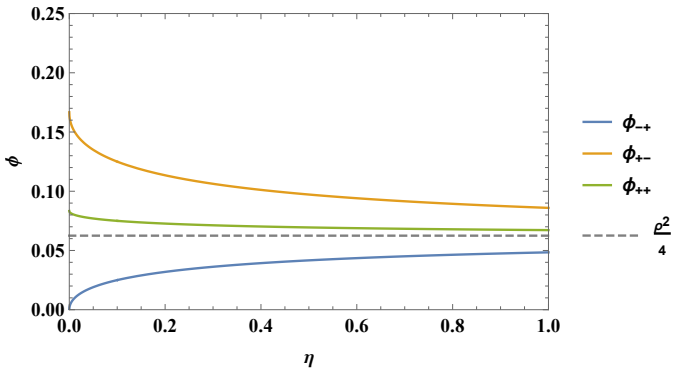

Figure 2: From up to bottom the PA predictions for $\phi_{++}, \phi_{+-}, \phi_{-+}$, as a function of η at fixed $\rho = 0.5$. The dashed line is the asymptotic uncorrelated value $\frac{\rho^2}{4}$ that the marginals reach at $\eta \to \infty$

stationary state , we have

$$\begin{aligned} J_+ &= \mathbb{P}\left[n_i = 1, n_{i+1} = 0\right] = \\ &= \mathbb{P}\left[n_i = 1\right] - \mathbb{P}\left[n_i = 1, n_{i+1} = 1\right] - \mathbb{P}\left[n_i = 1, n_{i+1} = -1\right] = \\ &= \frac{\rho}{2} - \phi_{++} - \phi_{+-} \end{aligned} \tag{53}$$

- In order to use (29) to evaluate l_c, first it is needed to approximate the probability to find a cluster of size l at some lattice site (26)

$$\begin{aligned} P_s(l) &\approx \frac{\mathbb{P}\left[n_0 = 0, n_1 \neq 0\right] \prod_{i=1}^{l-1} \mathbb{P}\left[n_i \neq 0, n_{i+1} \neq 0\right] \mathbb{P}\left[n_l \neq 0, n_{l+1} = 0\right]}{\prod_{j=1}^{l} \mathbb{P}\left[n_j \neq 0\right]} = \\ &= \sum_{\{s_i = \pm\}_{i=1}^{l}} \frac{1}{\prod_{i=1}^{l} \rho_{s_i}} \left(\rho_{s_1} - \phi_{+s_1} - \phi_{-s_1}\right) \left(\prod_{i=1}^{l-1} \phi_{s_i, s_{i+1}}\right) \left(\rho_{s_l} - \phi_{s_l +} - \phi_{s_l -}\right) = \\ &= \left(\frac{2}{\rho}\right)^l \begin{pmatrix} \frac{\rho}{2} - \phi_{++} - \phi_{-+} \\ \frac{\rho}{2} - \phi_{+-} - \phi_{++} \end{pmatrix}^T \begin{pmatrix} \phi_{++} & \phi_{+-} \\ \phi_{-+} & \phi_{++} \end{pmatrix}^{l-1} \begin{pmatrix} \frac{\rho}{2} - \phi_{++} - \phi_{+-} \\ \frac{\rho}{2} - \phi_{-+} - \phi_{++} \end{pmatrix} \end{aligned} \tag{54}$$

where in the last step $\rho_+ = \rho_- = \frac{\rho}{2}$ and $\phi_{--} = \phi_{++}$ have been used. Now the same procedure carried out in the previous section leads to:

$$\begin{aligned} P_s(l) = \\ = &\frac{2^{l-3}\rho^{-l}}{\sqrt{\phi_{-+}\phi_{+-}}} \Bigg\{ \left(\sqrt{\phi_{-+}} + \sqrt{\phi_{+-}}\right)^2 \left(\sqrt{\phi_{-+}\phi_{+-}} + \phi_{++}\right)^{l-1} \left[\rho - 2\left(\phi_{++} + \sqrt{\phi_{-+}\phi_{+-}}\right)\right]^2 + \\ &- \left(\sqrt{\phi_{+-}} - \sqrt{\phi_{-+}}\right)^2 \left(\phi_{++} - \sqrt{\phi_{-+}\phi_{+-}}\right)^{l-1} \left[\rho - 2\left(\phi_{++} - \sqrt{\phi_{-+}\phi_{+-}}\right)\right]^2 \Bigg\} \end{aligned} \tag{55}$$

$$\sum_{l=1}^{\infty} P_s(l) = \rho - \phi_{+-} - 2\phi_{++} - \phi_{-+} \qquad \sum_{l=1}^{\infty} l P_s(l) = \rho$$

the probability of finding a cluster of any size at a lattice site correctly sums up to ρ, the prob of finding a particle. In the end the average cluster size is obtained from equation (29), giving the PA prediction

$$l_c = \frac{\rho}{\rho - \phi_{+-} - 2\phi_{++} - \phi_{-+}} \tag{56}$$

- The gap size distribution can be obtained with the same reasoning used for the distribution of the cluster sizes $P_c(l)$. Starting from the the of finding a gap of size m at a given site, we can write the probability that a gap has a size m:

$$Q_c(m) = \mathbb{P}\left[\text{find a gap of size } m | \text{find a gap}\right] = \frac{\mathbb{P}\left[\text{find a gap of size } m\right]}{\mathbb{P}\left[\text{find a gap}\right]} \tag{57}$$

The approximation comes in place when writing the probability over sites $Q_s(m)$, in a similar way to equation (54), giving:

$$\begin{aligned} Q_s(m) &= \mathbb{P}\left[n_0 \neq 0, n_1 = 0, ...n_m = 0, n_{m+1} \neq 0\right] \approx \\ &\approx \frac{\mathbb{P}\left[n_0 \neq 0, n_1 = 0\right] \prod_{i=1}^{m-1} \mathbb{P}\left[n_i = 0, n_{i+1} = 0\right] \mathbb{P}\left[n_m = 0, n_{m+1} \neq 0\right]}{\prod_{j=1}^{m} \mathbb{P}\left[n_j = 0\right]} = \\ &= \sum_{s_0, s_{m+1} = \pm} \left(\rho_{s_0} - \phi_{s_0 +} - \phi_{s_0 -}\right) \left(\rho_{s_{m+1}} - \phi_{+ s_{m+1}} - \phi_{- s_{m+1}}\right) \times \\ &\qquad \times \frac{\left(1 - \rho_+ - \rho_- - \rho_+ + \phi_{++} + \phi_{-+} - \rho_- + \phi_{+-} + \phi_{--}\right)^{m-1}}{(1 - \rho_+ - \rho_-)^m} = \\ &= (\rho - \phi_{+-} - 2\phi_{++} - \phi_{-+})^2 \frac{\left(1 - 2\rho + \phi_{+-} + 2\phi_{++} + \phi_{-+}\right)^{m-1}}{(1-\rho)^m} \end{aligned} \tag{58}$$

this is valid for all $m \geq 1$. The probability of finding a gap is obtained by summing $Q_s(m)$ from 1 to ∞. Substituting into equation (57), the gap size distribution is obtained:

$$\begin{aligned} Q_c(m) &= \frac{Q_s(m)}{\sum_{n=1}^{\infty} Q_s(n)} = \\ &= \left(\frac{1 - 2\rho + \phi_{+-} + 2\phi_{++} + \phi_{-+}}{1 - \rho}\right)^m \frac{1 - \frac{1}{1-\rho}\left(1 - 2\rho + \phi_{+-} + 2\phi_{++} + \phi_{-+}\right)}{\frac{1}{1-\rho}\left(1 - 2\rho + \phi_{+-} + 2\phi_{++} + \phi_{-+}\right)} = \\ &= \left(\frac{1 - 2\rho + \phi_{+-} + 2\phi_{++} + \phi_{-+}}{1 - \rho}\right)^{m-1} \left[\frac{\rho - \phi_{+-} - 2\phi_{++} - \phi_{-+}}{1 - \rho}\right] \end{aligned} \tag{59}$$

Its average is:

$$\sum_{m=1}^{\infty} m Q_c(m) = \frac{1 - \rho}{\rho - \phi_{+-} - 2\phi_{++} - \phi_{-+}} = \frac{L - N}{N} l_c \tag{60}$$

With these tools, we will discuss the predictions in section 2.3.

2.2.2 Numerical Integration and Phase Separation

Equations (44) have been numerically integrated using the built-in functions given in Mathematica, that allow to solve systems of differential equations, so that all $6L$ marginals are obtained as functions of time. The initial conditions were defined by deciding a profile (the values assumed by a quantity over the lattice) for $\rho^0_{+,i}$ and $\rho^0_{-,i}$, such that $\rho^0_{+,i} + \rho^0_{-,i} < 1 \ \forall i$, in this way the probabilities cannot go above 1 and equations do not stumble upon singularities during the integration (the densities appear in denominators). The pair marginals at $t = 0$ were obtained as products of single-site ones for simplicity, in any case the stationary state should not depend in a relevant way on this particular choice.
The stability of the profiles at $t = T$, obtained by the integration has been verified by linearizing the system of equations (44) and studying the coefficient matrix of the resulting differential equation. In fact (44), if we consider the collection of the marginals $x = \left\{\rho^t_{+,i}, \rho^t_{-,i}, \phi^t_{++,i}, \phi^t_{+-,i}, \phi^t_{-+,i}, \phi^t_{--,i}\right\}_{i=1}^{L}$, can be rewritten as $\frac{dx}{dt} = f(x(t))$, where $f(x)$ contains the expressions on the r.h.s. of (44) and the following matrix can be defined

$$M_{a,b} = \left.\frac{\partial f_a}{\partial x_b}\right|_{x = x_*} \tag{61}$$

If M is negative semi-definite then x_* is a stationary state that is stable, otherwise the fixed point is unstable, because positive eigenvalues appear and some perturbation can bring the system to another state.

What appears from the integrations is a behavior that is not observed in the simulations of the model. These show that the system reaches a uniform stationary state for all values of the parameters, and all initial conditions, with clusters that can evaporate and form everywhere in the lattice, on the other hand the PA seems to describe a phase separation: when the tumble rate is low enough the stationary profile of all quantities is inhomogeneous, with regions that are at a constant density of particles which can be higher or lower then the total density $\rho = \frac{N}{L}$. Examples of these kind of profile for different values of η are shown in figure 3, these data are obtained starting the integration from a profile where the lattice is half filled ($\rho = 0.5$), with the particles concentrated in one half of the lattice. Using values of $\eta \geq 0.04$ the phase separation is not observed anymore. Another observation is that the values of the pair marginals where the density is constant seems to satisfy the relations $\phi_{++}(\eta, \rho), \phi_{+-}(\eta, \rho), \phi_{-+}(\eta, \rho)$ obtained by solving the system of equations (51).

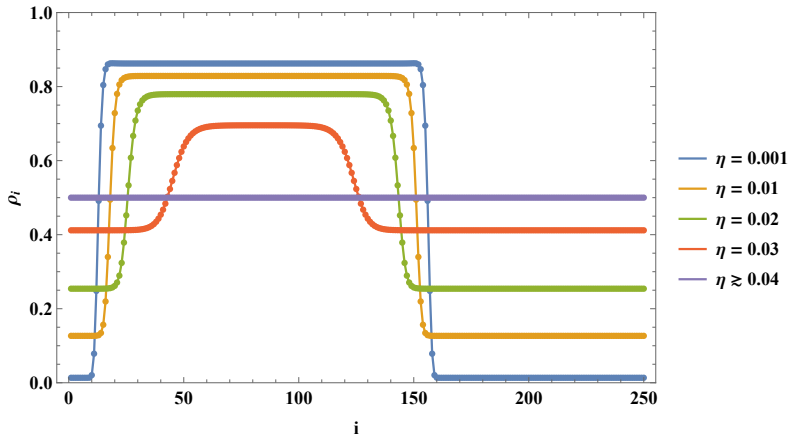

Figure 3: Profiles of the density $\{\rho_i\}_{i=1}^{L}$, for mean density $\rho = 0.5$ and some values of the tumble rate. obtained by numerically integrating the pair approximated dynamical equations up to time $T = 5 \times 10^6$ time units

The uniform profile is always a fixed point of equations (44) since a solution to the system (51) can always be found. The results show that if the integration starts with the density profile such that $\rho_{\pm,i} = \frac{\rho}{2}$, then the only evolution that can be observed is the relaxation of the pair marginals to the values predicted by equations (51), this has been tested for many values of η. What changes is the stability of this profile. By numerically evaluating the spectrum of M, using the uniform configuration in place of x^*, one can see that it becomes unstable for $\eta \lesssim 0.04$, the spectrum of M acquires some eigenvalues ν with positive real part, on the other hand the same evaluation done using the inhomogeneous stationary configurations seems to show that they are stable (eigenvalues with positive real parts are present but they are negligible with respect to the real part found for the uniform solution, and they appear to become smaller by increasing L or reducing η). A plot of the eigenvalues in the complex plane for a stable configuration and a uniform one when $\eta = 0.01$ can be found in figure 4. By numerically evaluating the eigenspace S associated to one of these ν it can be found that $dim(S) = 2$ and the eigenvectors have a sinusoidal profile in space, with a wavelength that is a fraction of L and changes depending on the considered ν. If one considers that the new inhomogeneous stable stationary states (ISSS) present the alternation of regions at high and low densities and ISSS with a number of cluster regions greater than 1 seem to be possible, it is possible to speculate that each ν corresponds to the possible relaxations to a family of fixed points characterized by a common shape that can produce L profiles by translating the shape on the lattice.

We mention that the appearance of ISSS with more than one high density region can be obtained with certain initial conditions and values of the parameters η and ρ, but they most often happen to be transient states that undergo abrupt coalescence processes after periods characterized by small

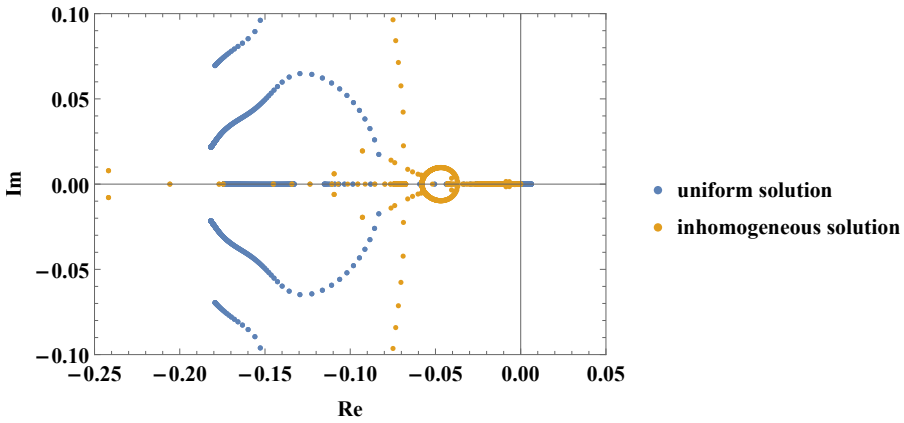

Figure 4: Plot of the eigenvalues of the coefficient matrix M for $\eta = 0.01, \rho = 0.5, L = 500$, for an inhomogeneous state and the stationary homogeneous state, zoomed out in the region near the origin where the eigenvalues with positive real part appear. The eigenvalues with maximum real part are $0.006 + 0i$ for uniform, $8.9 \times 10^{-11} + 0i$ for the inhomogeneous profile.

variations. Also the position of the high density region depends on the initial state of course.
This phenomenon described by the PA has no match with the simulations since, as it is expected, there is no trace of breaking of the translational symmetry at stationarity, independently of the starting state. Even if the system is prepared with all the particles close to each other to form a cluster, this configuration lasts a time $\sim \eta^{-1}$, and time averages do not suggest the existence of the local stability of an high density region. For this reason the ISSS have not been further explored and better characterized in this work.
Nonetheless some considerations can be made on this behavior of the PA applied to the PEP on a 1D chain. Many studies have conjectured that a mobility induced phase separation (MIPS) could happen in active systems with run and tumble particles [CT15]. The study [MRM23] has argued that a phenomenon of this type is not possible in the 1D PEP. Summarizing the paper, it considers a model analogous to the PEP characterized by a lower mobility of particles for which an exact solution is available. Since the MIPS does not happen in the aforementioned system then it can be argued that it cannot happen in the PEP.
The same wrong behavior of the PA appears if one solves the MF equations at stationarity [Cat12], and it can be observed that the critical value of η seems to get smaller in the PA. From this it is possible to speculate that this phenomenon could disappear for more refined mean field cluster approximation (the class of approximations to which MF and pair belong, that use respectively "clusters" of size 1 and 2), with the critical η tending to 0 as the size of the cluster increases. This can be seen in figure 5 where the difference between the stationary state obtained by numerical integrations is compared with the homogeneous solution, this is done by evaluating:

$$d = \sqrt{\sum_{i=1}^{L} \left(\rho_i - \frac{N}{L}\right)^2} \tag{62}$$

the difference becomes zero for $\eta \approx 0.1$ in the case of the MF and for $\eta \approx 0.03$ in case of the PA. A more rigorous proof of this reduction could be obtained by searching the value of η for which the homogeneous stationary state becomes unstable, but this goes beyond the scope of this work.
In general, it can happen that MF cluster approximations, for small clusters, capture phase transitions that are present at dimensionalities higher than 1, because it cannot take into consideration the shape of the lattice.
Another consideration can be done, it is based on the fact that there is the possibility to restore the

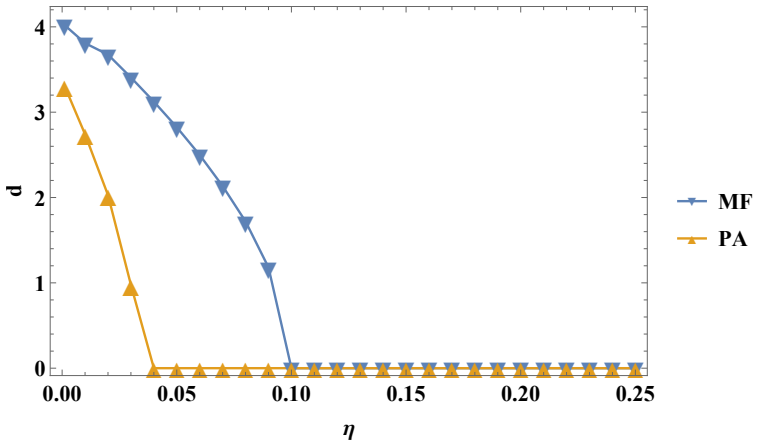

Figure 5: Euclidean distance between the (assumed) stationary density profile ρ_i obtained from numerical integrations and the uniform density $\rho = \frac{N}{L} = 0.5$, for different values of η. Integrations started with the system half-filled. System size $L = 250$

translational symmetry of the ISSS by performing an averaging of the profile over the sites, obtaining values of $\{\phi_{++}, \phi_{+-}, \phi_{-+}\}$ that are different by the ones obtained from (51) at equal total density ρ. This can be regarded as averaging of the stationary profiles with respect to the initial states. For this reason in order to carry out this average in a more rigorous way, one should average over sites and over the possible ISSS that it is possible to obtain for some η and ρ, using weights that reflect how likely it is to obtain a given shape of the stationary profile. In absence of a way to enumerate all the possible ISSSs in a controllable way (even for fixed parameters), and evaluate the weights, here we will give some results obtained by averaging only on the ISSSs with one cluster region, just to have an example of how this operation improves the PA predictions for the pair marginals at low tumble rates. These results are present in the next section 2.3, figure 7.

2.3 Comparing the methods

In this section we will compare the results of the two different MF theories to mean-field that have been used to approximately describe the PEP: the first one can be regarded as an example of so-called particle-oriented mean-field (POMF) approximations [SS97], whereas the pair approximation falls in the family of the cluster methods that are instead site-oriented MF approximations [bK92]. The difference between the two methods is in the variables used to describe the state of the system, in the former case the distances between particles $\{m_k\}_{k=1}^{N}$ are used and they are assumed to be uncorrelated, in the latter case the variables are the sites occupations $\{n_i\}_{i=1}^{L}$ and correlations are neglected between sites at a distance greater then one. So here we are making a comparison between these two approaches to MF.
The approximation presented in subsection 2.1 is not a simple particle oriented MF because the size of the gaps are conditioned on the internal states of both particles at the end of the gap, while usually this method has been used on traffic models where particles move in one direction (the method is also regarded as car oriented mean field) and so the conditioning is usually done on the internal state of the particle at the left end of the gap:

$$P\left(\{m_k\} \mid \{s_{k+\frac{1}{2}}\}\right) \approx \prod_k P\left(m_k \mid s_{k+\frac{1}{2}}\right)$$

This was the approach in the study [PG13], on the pausing TASEP (pTASEP) where particles can go in a motionless state, in the same way as in the PEP particles can change direction. In the PEP the conditioning done in this way would have been not so reasonable considering its left-right symmetry, where no preferred direction of motion exists and so both particles at the end of a gap affect it in the same way.
Both approximations, site oriented and particle oriented, underestimate the clustering phenomenon.

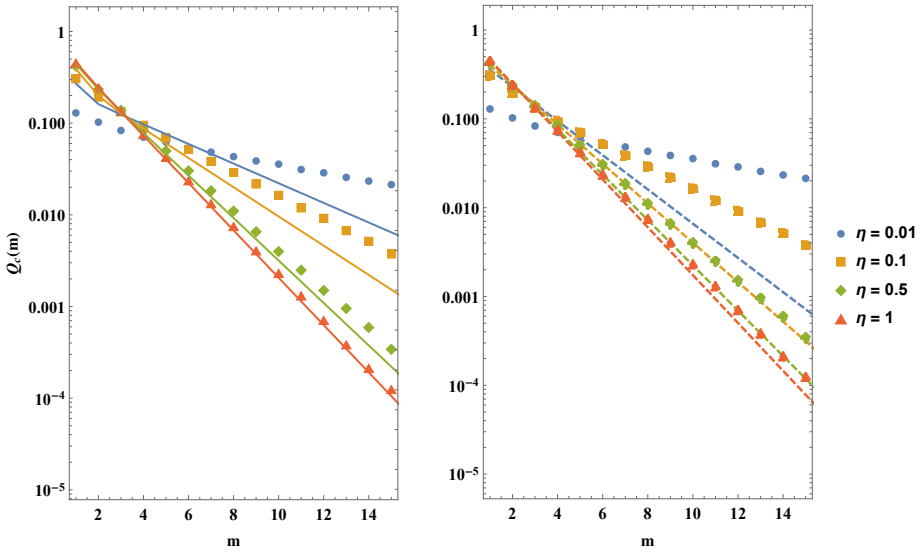

(a) Symbols: simulations. Solid lines: MF mass model predictions

(b) Simbols: simulations. Dashed lines: PA predictions

Figure 6: Gap size distributions $Q_c(m)$ for some η. Comparison of the approximations with the simulated values obtaines for $\rho = 0.5$. Simulations done with $L = 1000$.

Clusters are temporary structures whose life and size increase for smaller η values, so they tend to correlate particles. Neither PA nor POMF are able to fully capture this mechanism: PA tries to describe just the nearest-neighbor correlations, while the MF mass model tries to describe the behavior of gaps between particles but still neglects correlations beyond particle pairs. The latter method ends up giving better predictions, this could mean that clusters that correlate particles at large distances end up correlating also the vacancies. The MF mass model is able to well capture this, very well when η approaches 1, while the PA underestimates the probability of having large gaps for all values of η. This can be seen in figure 6, where the predictions of the two approximations are compared with statistics of gaps obtained from simulations, and it is possible to see that the MF mass model does a better job in describing how the exponential decay of the gap distribution changes with η. The mass distribution P_m, given in equation (21), cannot be directly compared with $Q_c(m)$, instead one has to consider:

$$\frac{P_m}{1-P_0} \qquad \text{for} \quad m \geq 1 \tag{63}$$

where $\sum_{m=1}^{\infty} P_m = 1 - P_0 = \frac{4-\alpha-2\beta-\delta}{4}$ is written in terms of spin conditioned probabilities defined in equation (8).
While P_m is defined for $m \geq 0$, while the distribution of gaps sizes $Q_c(m)$ is defined for $m \geq 1$ (see equation (57)) because the probability is conditioned to having found a gap, and corresponds to how statistics are done in simulations where sequences of empty sites are counted.

Let us continue by comparing the predictions for the pair marginals at stationarity. In the mass model the probabilities are defined over particles so to compare them with the pair marginals, which are defined over sites, we need to observe that:

$$\mathbb{P}[n_i = \sigma, n_{i+1} = \sigma'] = \mathbb{P}[n_i = \sigma]\,\mathbb{P}[n_{i+1} = \sigma' | n_i = \sigma] = \frac{N}{L}\mathbb{P}\left[m_k = 0; s_{k-\frac{1}{2}} = -\sigma, s_{k+\frac{1}{2}} = -\sigma'\right] \tag{64}$$

so that $\phi_{++}, \phi_{+-}, \phi_{-+}$ will be compared respectively with $\rho\,\beta, \rho\,\alpha, \rho\,\delta$. In figure 7 this comparison has been done by varying ρ while considering a fixed value of tumbling rate, $\eta = 0.01$, which is

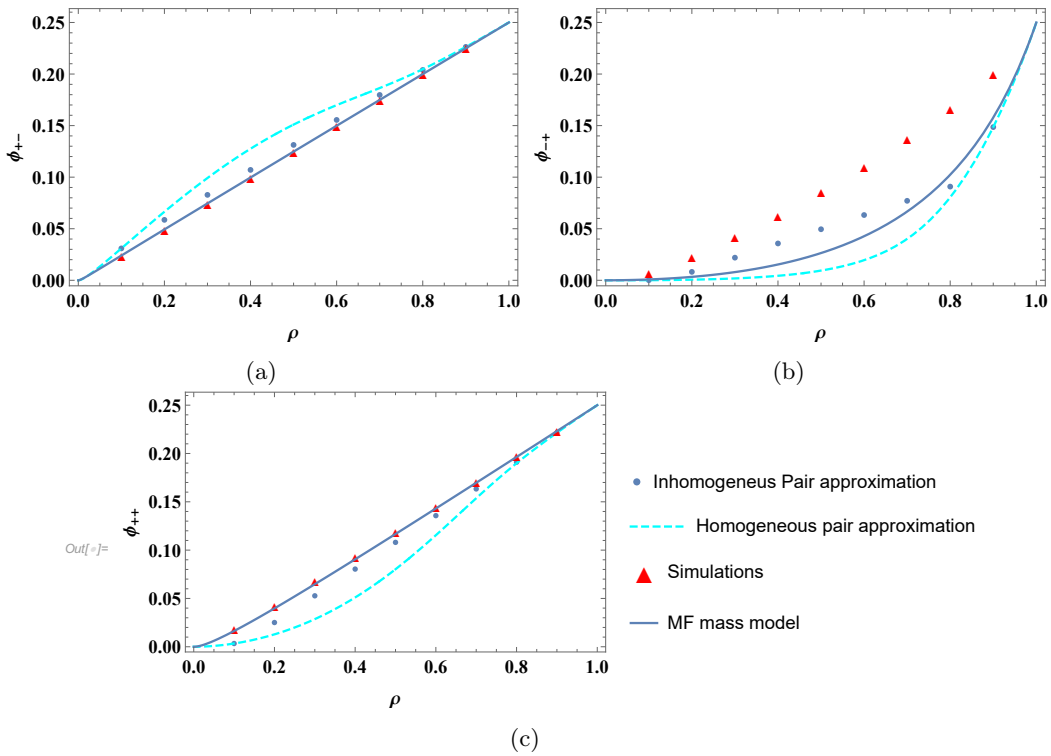

Figure 7: Plots of pair marginals $\phi_{++}, \phi_{+-}, \phi_{-+}$ as a function of ρ at fixed $\eta = 0.01$. Comparison of the approximated predictions from MF mass mode, homogeneous PA, inhomogeneous PA with the simulated values

a value at which clustering is important and η^{-1} is not comparable with the system size L. The figure also includes values of the pair marginals obtained from simulations and the predictions of $\phi_{++}, \phi_{+-}, \phi_{-+}$ obtained by averaging an inhomogeneous stationary profile. From the graphs it can be seen that both POMF and PA tend to overestimate the pair marginal $[+-]$ (the POMF does it slightly), and underestimate the marginals $[-+]$ and $[++]$. The largest discrepancies are in the predictions of ϕ_{-+}. Let us look at the structure of the equation for dynamical evolution of this pair marginal in both approximations, equation (48) and equation (13) in the case $m = 0$: at stationarity and with small η, the term due to the tumble is not compensating the negative terms that describe the particles moving away from each other.

When $\eta \ll \lambda$, it happens in the simulations that most of the particles are in clusters and only a small fraction is moving, inside a cluster the orientations of particles are random and are continuously shuffled by the tumble dynamics, so these particles contribute to the pair marginals that we are considering with a term $\frac{\rho}{4}$, since if a particle is found inside a cluster it will have for sure another particle near it and the probability to find them with given orientations is $\frac{1}{2} \times \frac{1}{2}$. This is captured by the MF mass model, for $[+-], [++]$, and it is remarkable, the problem is that the various $P_m^{ss'}$ decay more slowly at large m in simulations [DCR20].

At the border of the clusters it is most probable to find two particles that point toward the cluster, so that they prevent other particles from leaving the cluster. Conversely, particles moving in the regions between clusters do not contribute much to the probabilities of configurations $[++], [-+]$, because they can form these structure only temporarily when they are close to one anothr. Configuration $[+-]$ is different because, when two moving particles collide to form it, this structure will last until one of the two particles tumbles, unless other particles collide and in this case the cluster will start to grow.

The above considerations for the behavior at small η are directly reflected in the predictions of the observables given by the approximations. The expressions of the current, in equation (53) and

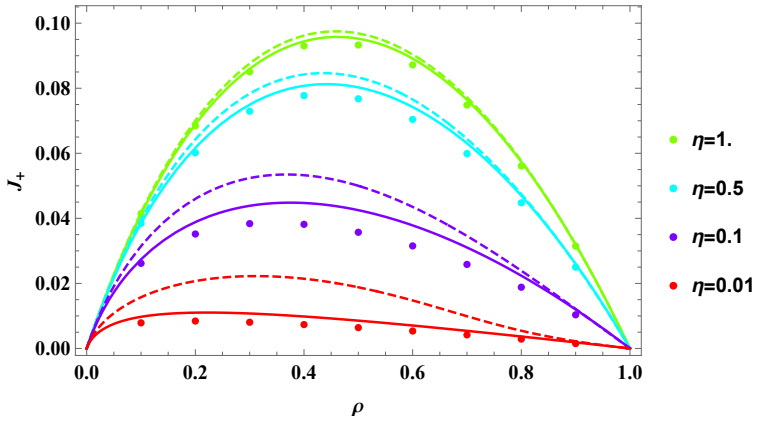

Figure 8: Fundamental diagram of the PEP $J_+(\rho)$ predictions vs simulations for various tumble rates η. The dots are obtained by simulations, the solid line is the MF mass model, the dashed line is given by the pair approximation

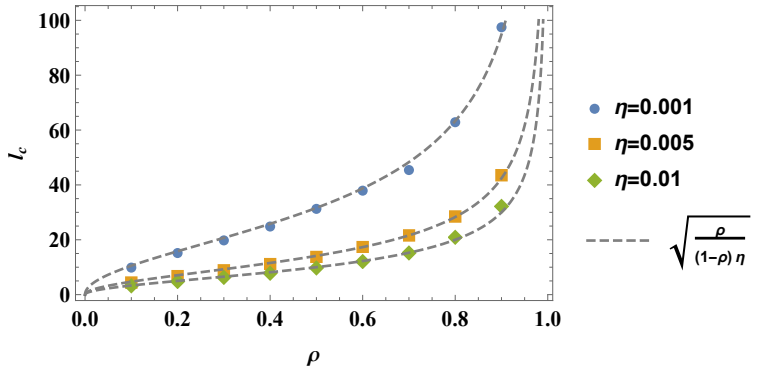

Figure 9: Average cluster size l_c as a function of ρ and some small values of η Symbols are simulations of the PEP done with L=1000, with 7500 samples taken on the same simulated system at time intervals $\Delta t \sim \frac{1}{\eta}$. Dashed line is the scaling (29).

equation (25), do not contain the probability ϕ_{-+}, so the approximation for this quantity ends up not so far from the simulated results. This can be seen in figure 8, where one can appreciate the greater accuracy of the MF mass model, as well as the fact that there is good qualitative matching, even though the approximations always overestimate the current, which is the same as saying that they overestimate the amount of particles that are not in a cluster.

The average cluster size l_c is a much less trivial quantity. While the current is a correlation between two adjacent sites, l_c depends on the probabilities of observing sequences of l particles in the system, see equation (26) and equation (29), so it is expected that approximations give poor results in regimes where particles are highly correlated.

A general expression for l_c is not available, but we have the expression obtained in section 2.1.3 in the limit of $\eta \ll \rho$, when the behavior of particle clusters can be effectively described by an equilibrium process of growth and evaporation [SG14] [CMT23] and the average cluster size scales as

$$l_c \sim L_c = \sqrt{\frac{\rho}{(1-\rho)\eta}} \tag{65}$$

The match with simulations done at small tumbling rates can be seen in figure 9. All the simulated values of l_c shown here are obtained using the total number of clusters of size l obtained in all the samples:

$$l_c^{\text{sim}} = \sum_{l=1}^{\infty} l \frac{\sum_{\mathcal{C}\in\text{samples}} \#\{\text{clusters of size l in } \mathcal{C}\}}{\sum_{\mathcal{C}\in\text{samples}} \#\{\text{clusters in } \mathcal{C}\}} \tag{66}$$

the other possibility would have been to first average over l and then over sampled configurations, this is a conceptually different quantity because of the finiteness of the system, but we compared the values and they practically coincide, at least for the values of η that we consider. In general the

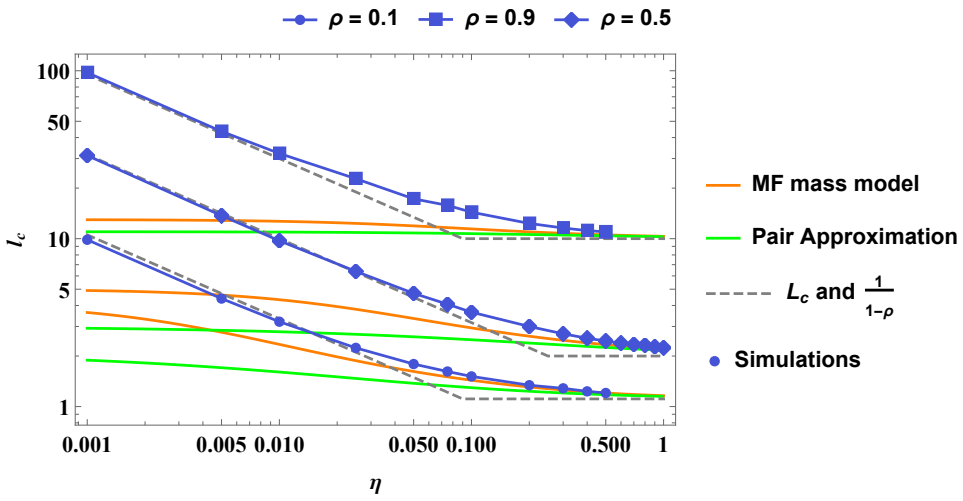

Figure 10: Logarithmic plot of the average cluster size l_c as a function of tumble rate η for three different values of the particle density ρ. Comparison of the predictions from various approximations against simulations. Simulations done for systems with lattice sizes $L = 1000$

size of the system is known to have effects on the cluster sizes [CMT23]. In figure 10, it can be seen that the approximations fail to capture the low η scaling (65) and become close to the simulations only for the higher values of η. The predictions approach the exact asymptotic result

$$l_c \xrightarrow{\eta\to\infty} \frac{1}{1-\rho} \tag{67}$$

This result was expected because the PEP becomes a symmetric exclusion process for $\eta \to \infty$ [DCR20], and this system has a probability measure of the stationary configurations that factorizes over sites:

$$P\left(\{n_i\}_{i=1}^{L}\right) = \prod_{i=1}^{L} P\left(n_i\right) \qquad P\left(n_i\right) = \begin{cases} \frac{\rho}{2} & \text{if} \quad n_i = \pm 1 \\ 1-\rho & \text{if} \quad n_i = 0 \end{cases} \tag{68}$$

substituting the latter in equation (26), and using it to evaluate the average cluster size (29), the result (67) is recovered.

From the results considered, it can be said that the MF mass model can be considered a refinement of the PA when describing the PEP, as it always gives better predictions for the pair marginals. The PA is less involved in the calculations and it has the possibility to be easily modified in the case of different BCs, while this would be much less trivial for the mass model, since the definition of the quantities relies on the fixed order of the particles. The mass model has no possibility to be used for systems with lattice dimensionality different from 1.

Numerically, the PA is easier to handle and it can be used to study the dynamical behavior of the finite system and how it reaches stationarity, as well as the behavior of the system when the translational invariance is not satisfied. The MF mass model presents the following complications if one wants to make numerical integrations:

- The system of dynamical equations, as it is written in eqs. (10)-(13), works only in the thermodynamic limit, to use them numerically a cut-off value for m has to be included, for example it can be $m_{\text{cut}} = L - N$, which is the maximum value m can assume in a finite system. This is needed because an infinite system of equations cannot be defined on a computer, but in order to have a cut-off, the equations need to be modified to ensure that the normalization is conserved and that ρ_{mass} is conserved;

- Another complication is that the stationary $P_m^{ss'}$ reach really small values quickly with m, and numerically this can become a problem;
- When considering the inhomogeneous case, it occurs that the number of degrees of freedom grows quadratically in the system size L, assuming a number of particle N that is proportional to L and $m_{\text{cut}} = L - N$:

$$\#\, of\ variables = 4Nm_{\text{cut}} \sim L^2$$

which is quite worse then the linear growth of the PA.

3 Generalized Persistent Exclusion Process

Before introducing the generalized model we briefly review the phenomenology of the simple TASEP, with a focus on the phase diagram of the OBCs system.

3.1 Totally Asymmetric Simple Exclusion Process

The Totally Asymmetric Simple Exclusion Process, can be considered among the simplest possible stochastic transport models. First introduced to describe transport inside cells, where molecular machines are able to perform motion and are kept running through mechanochemical reactions, this model has later become important in physics, where it has become paradigmatic for nonequilibrium and modeling of traffic problems, with many available results.
Details on the TASEP, exact results and some variations of the model, can be found in the dedicated chapter of the book [SCN11]. For additional details on the exact solution and the OBCs phase diagram can be found in the TASEP section of [Sch01]. The present description is a short resume without derivations, containing some minimal ideas, the ones we need as references for describing the behaviors of systems with open boundary conditions at stationarity, so that we will be able to discuss a richer model with some fixed concepts.
The TASEP is a driven diffusive model where particles live on a one-dimensional lattice with L sites, their motion is totally asymmetric because they move in one direction, say from left to right, with the restriction that a site cannot be occupied by more than one particle. The latter rule is the exclusion interaction. Each particle independently attempts to make a step forward with rate λ, so we are considering the sequential update version of the model, as we do for all the other models throughout this thesis. In the OBCs version of the model a particle can enter at site 1 if the latter is empty, while a particle at site L can leave the lattice, it is customary to call the rates of these two processes respectively α and β, respectively, not to be confused with the α and β symbols introduced in section 2. This is totally analogous to having reservoirs at the two ends of the system, with densities[3]

$$\rho_0 = \frac{\alpha}{\lambda} \qquad\qquad \rho_{L+1} = \frac{1-\beta}{\lambda}$$

Time can be rescaled to make λ unitary without loss of generality.
In describing the phenomenology of the stationary state we will consider the current at stationarity, that we call J, and that is the main quantity characterizing a phase. We will also describe the stationary density profile $\{\rho_i\}_{i=1}^L$, which is the collection of the probabilities of finding a particle at each site. The density profile can be roughly divided into three regions, two near the boundaries and a central one that constitutes the bulk of the lattice.
In a uniform density profile, J is determined by the density ρ through the relation:

$$J = \rho(1-\rho) \tag{69}$$

This is the fundamental diagram of the model, which can be obtained by studying the TASEP with periodic boundary conditions, on an infinite lattice. It tells us that particles in this ideal situation, become uncorrelated at stationarity.

[3]The fact that α and β must be constrained in order to keep the reservoir densities between 0 and 1 turns out to be irrelevant to the physics of the system.

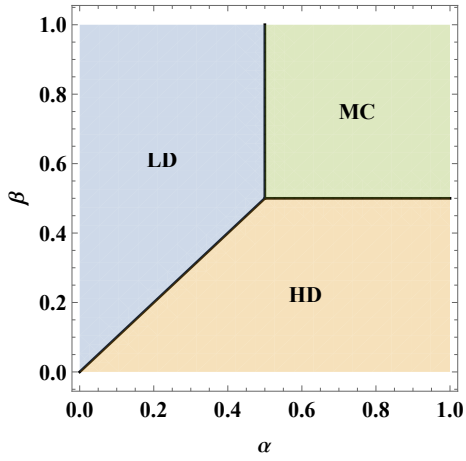

Figure 11: Phase diagram of the TASEP in the α-β plane

Another important relation between densities and currents is the continuity equation, which can be obtained by studying the master equation of the model

$$\frac{\mathrm{d}\rho_i^t}{\mathrm{d}t} = J_{i-1}^t - J_i^t \qquad \text{for} \qquad i = 1, ..., L \tag{70}$$

where the currents have the following expressions with OBCs

$$J_i^t = \begin{cases} P_i^t[1,0] & \text{for} \quad i = 1, ..., L-1 \\ \alpha P_1^t[0] & \text{for} \quad i = 0 \\ \beta P_L^t[1] & \text{for} \quad i = L \end{cases} . \tag{71}$$

The notation introduced in (41) has been used.
At stationarity the system can be in three distinct phases, that appear because the current throughout the lattice must be uniform, according to equation (70) when time derivatives vanish, and it can be said that there are three ways in which J can be limited, each leading to a phase:

- when the left boundary limits the inflow, the system is in the low density(LD) phase;
- when the right boundary limits the outflow, the system is in the high density(HD) phase;
- when the transport is limited by the bulk hopping, then the system is in the maximum current(MC) phase.

These three statements are enough to have an intuition on why the three phases come in place, but there is actually a non-rigorous argument that is able to describe the behavior of the system, and the regions of the phase diagram. It is a picture that uses the diffusion of domain walls and the propagation of localized perturbations, described both in [SCN11] and [Sch01]. The regions of the α-β plane associated to each stationary phase can also be obtained in the MF approximation, by solving the system of equations resulting from the approximation of equation (70). It is the same phase diagram obtainable in the domain wall picture and in the exact solution of the model. We proceed to give a brief characterization of the phases that we report in figure 11.

3.1.1 Low Density Phase ($\alpha < \frac{1}{2}$, $\alpha < \beta$)

When $\alpha < \frac{1}{2}$ and $\alpha < \beta$, the left reservoir controls the system. The current is equal to

$$J = \alpha(1 - \alpha) \tag{72}$$

The density ρ_i is constant (in the limit $L \to \infty$) at the left end of the system and throughout the bulk with the same value of the input reservoir, so that a density of the bulk can be identified:

$$\rho_{\text{bulk}} = \rho_0 = \alpha \tag{73}$$

At the right end the density smoothly varies from ρ_{bulk} to $\rho_{L+1} = 1 - \beta$, giving rise to a boundary layer(BL). The density in the BL decays exponentially to the value of the bulk.
Both J and ρ_{bulk} are determined solely by the injection rate α, this is why it can be said that the LD is input controlled, β can only have a role in defining the length scale over which the BL develops, which occupies a finite part of the infinite lattice.

3.1.2 High Density Phase ($\beta < \frac{1}{2}$, $\beta < \alpha$)

When $\beta < \frac{1}{2}$ and $\beta < \alpha$, the right reservoir controls the system. The behavior in this phase follows from the one of the LD phase if one considers the particle-hole symmetry of the TASEP: holes behave as particles moving leftward throughout the lattice, with the same rules of actual particles and the roles of the boundaries interchanged, holes exit at the left boundary with rate α and enter at the right with rate β. The results for the HD phase can be obtained by performing the following substitutions:

$$\rho_i \to 1 - \rho_{L+1-i} \qquad \alpha \leftrightarrow \beta$$

So the current and the bulk density become

$$J = \beta(1 - \beta) \tag{74}$$

$$\rho_{\text{bulk}} = 1 - \beta \tag{75}$$

The density profile is uniform at the right end and throughout the bulk and the boundary layer forms at the left end.

3.1.3 Maximum Current Phase ($\alpha > \frac{1}{2}$, $\beta > \frac{1}{2}$)

When both α and β become larger than $\frac{1}{2}$, the current reaches the maximum value of the fundamental diagram $J_{\text{MAX}} = \frac{1}{4}$. The average current of particles on the lattice does not exceed this value. It is said that the bulk is controlling the phase because the boundaries play no role in defining the main physical quantities that instead depend on the limited transport of particles in the bulk. The quantities of interest in this case assume values:

$$J = \frac{1}{4} \qquad \rho_{\text{bulk}} = \frac{1}{2}$$

The density profile in this case has BLs at both ends of the chain, the density decays from the bulk value with a power-law behavior[4].
The current changes continuously when crossing all transition lines of the phase diagram. It follows eqs. (72), in the LD phase, and (74), in the HD phase, (the equations are equal on the line $\alpha = \beta$) until α or β reach the threshold value $\frac{1}{2}$, after which it stops growing and it becomes constant with $J = J_{\text{MAX}}$.

3.2 Generalized Model

In order to obtain a generalization of the TASEP that includes the PEP as a specific case we consider a model with two particle species, or states, with the possibility of changing between state 1 and state 2 through a process that will be called tumble even if the two types of particles could be moving in the same direction, and the tumbling rate notation will again be η. The model includes the exclusion interaction between particles, so that they can hop only if the arrival site is empty.

[4]In simulations $\rho_{\text{bulk}} = \frac{1}{2}$ can only be found at site $i = \frac{L}{2}$ because really large sizes are needed to fully develop a BL with a power law decay.

The processes of injection and extraction will be interpreted as couplings with reservoirs of particles that maintain their occupation constant over time, as in the case of the ordinary TASEP. Particles can enter if the target site is empty; the target site depends on the motion direction as will be exemplified later.

We shall call α the probability to find a particle in the left reservoir and $1-\beta$ in the right reservoir,

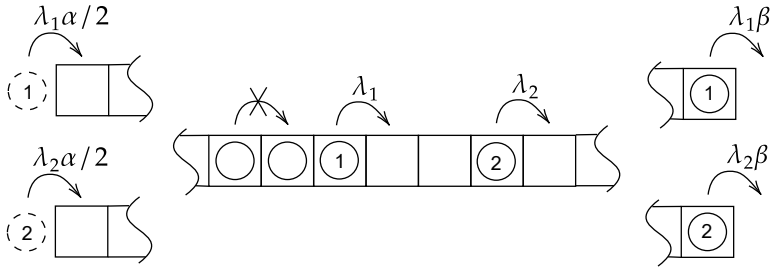

Figure 12: Pictorial representation of the generalized PEP when both particles species move in the same direction (i.e. rightward).

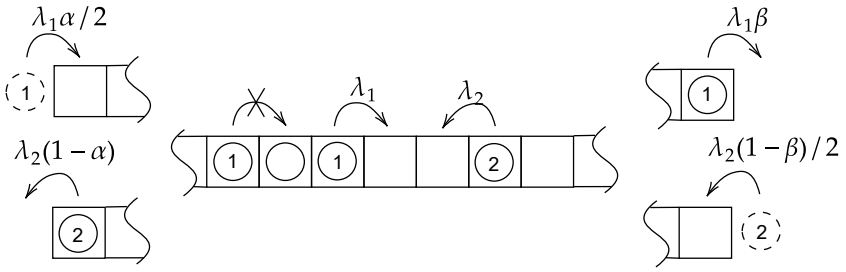

Figure 13: Pictorial representation of the generalized PEP with particles moving in opposite directions (i.e. species 1 rightward and species 2 leftward).

with equal amounts of particles of type 1 and 2 so that they enter with rate $\lambda_s\frac{\rho_\mathrm{R}}{2}$ and exit with rate $\lambda_s(1-\rho_\mathrm{R})$, where λ_s is the hopping rate of a particle of type $s=1,2$, and $\rho_\mathrm{R}=\alpha, 1-\beta$ is the occupation of the reservoir. The particles of type 1 always move in the positive (rightward) direction of the lattice, those of type 2 can move in positive or negative (leftward) direction, or stay still when $\lambda_2=0$. The boundary rates are explained in the following scheme:

- Type 1 always moving from left to right

$$\begin{cases} \lambda_1\dfrac{\alpha}{2} & \text{Left Boundary injection rate} \\ \lambda_1\beta & \text{Right Boundary extraction rate} \end{cases}$$

- Type 2 can move from left to right, right to left

$$\text{positive direction} \begin{cases} \lambda_2 \dfrac{\alpha}{2} & \text{Left Boundary injection rate} \\ \lambda_2 \beta & \text{Right Boundary extraction rate} \end{cases}$$

$$\text{negative direction} \begin{cases} \lambda_2(1-\alpha) & \text{Left Boundary extraction rate} \\ \lambda_2 \dfrac{1-\beta}{2} & \text{Right Boundary injection rate} \end{cases}$$

In case $\lambda_2 = 0$, the particles in state 2 do not move, so they cannot enter or exit the system, they only appear in the system through the tumble process. A pictorial representation of the processes occurring in the model has is given in figure 12 and figure 13. There was actually a lot of freedom available in the choice of the boundary conditions, for example the relative presence of particles of type 1 and type 2 or even the correlation between the injection and extraction of two consecutive particles, here the choice was taken in order to maintain the number of the parameters limited while trying to build up a model that resembles as much as possible a TASEP with reservoirs.
Indeed, from the point of view of the TASEP, this model describes the possibility that particles may assume a defective behavior during their motion for some time, restricting the flow of ordinary particles (i.e. the ones in state 1). For example, the case $\lambda_2 = 0$, the so-called pausing TASEP where particles can enter and exit a state where they do not move, may have some biological relevance in describing the effect of antibiotics [Kei+24], or some behaviors observed in Myosin motion [PG13].
The main quantity of interest will be the particle current at a given site of the lattice J_i evaluated at stationarity, defined in the following way:

$$J_i = J_{1,i} + J_{2,i} \tag{76}$$

where the definitions of the currents can be written using notation (41)

$$J_{1,i} = \lambda_1 P_i[1,0] \tag{77}$$

$$J_{2,i} = \begin{cases} \lambda_2 P_i[2,0] & \text{if particles in state 2 move rightward} \\ -\lambda_2 P_i[0,2] & \text{if particles in state 2 move leftward} \end{cases} \tag{78}$$

The latter definitions hold in the bulk ($1 \leq i < L$), while boundary currents have the expressions reported in Tables 1 and 2. For clarity J_i refers to the net current between the lattice sites i and $i+1$, whereas $J_{1,i}$ and $J_{2,i}$ are the contributions from particles in state 1 and 2, respectively.

Table 1: Boundary currents of fast particles (state 1)

Left boundary	Right boundary
$J_{1,0} = \lambda_1 \frac{\alpha}{2} P_1[0]$	$J_{1,L} = \lambda_1 \beta P_L[1]$

At stationarity, when the system falls in a state that is time invariant, J_i becomes independent of the position i on the lattice, because it has to satisfy the continuity equation for the density per site $\rho_i = \rho_{1,i} + \rho_{2,i}$

$$\frac{\mathrm{d}\rho_i}{\mathrm{d}t} = J_{i-1} - J_i \qquad \xrightarrow{\frac{\mathrm{d}}{\mathrm{d}t}=0} \qquad J_{i-1} = J_i = J$$

Where of course $\rho_i = \rho_{1,i} + \rho_{2,i}$ is the total density and $\rho_{s,i} = P_i[s] = \mathbb{P}[n_i = s]$ for $s = 1, 2$ are the single species densities. The continuity equation can be obtained by summing the two equations of the dynamical evolutions of the single species densities

$$\begin{cases} \dfrac{\mathrm{d}\rho_{1,i}}{\mathrm{d}t} = \eta(\rho_{2,i} - \rho_{1,i}) + J_{1,i-1} - J_{1,i} \\ \dfrac{\mathrm{d}\rho_{2,i}}{\mathrm{d}t} = \eta(\rho_{1,i} - \rho_{2,i}) + J_{2,i-1} - J_{2,i} \end{cases} \qquad \forall i \in \{1, ..., L\} \tag{79}$$

Table 2: Boundary Currents of slow particles (state 2)

	Left boundary	Right boundary
state 2 particles move rightward	$J_{2,0} = \lambda_2 \frac{\alpha}{2} P_1[0]$	$J_{2,L} = \lambda_2 \beta P_L[2]$
state 2 particles move leftward	$J_{2,0} = -\lambda_2(1-\alpha) P_1[2]$	$J_{2,L} = -\lambda_2 \frac{1-\beta}{2} P_L[0]$
state 2 particles do not move	$J_{2,0} = 0$	$J_{2,L} = 0$

From the latter equations it is easy to see that, even at stationarity, the single species currents have the possibility to vary over lattice sites if $\rho_{1,i} \neq \rho_{2,i}$, as for example it may happen at the boundaries of the system, with the following constraint

$$\eta(\rho_{1,i} - \rho_{2,i}) = J_{1,i-1} - J_{1,i} = -(J_{2,i-1} - J_{2,i}) \tag{80}$$

The importance of the current for the OBCs system considered here comes from the fact that, in the TASEP, the study of how J depends on the boundary rates is sufficient to outline the phase diagram in the α-β plane.
Some considerations can be made to reduce, as much as possible, the range of values that needs to be explored in the parameter space $\{\alpha, \beta, \eta, \lambda_1, \lambda_2\}$. First of all the jump rate of particles in state 1 can be taken as reference for the time scale and so from now on it will be $\lambda_1 = 1$. The other hopping rate λ_2 will always be smaller then 1 because we want to consider the particles in state 1 always the fast ones. To distinguish between the cases of particles moving in the same direction and in opposite directions we will refer to v_2, the average velocity of a single state 2 particle on the lattice, which corresponds to the hopping rate λ_2 with the sign of the motion direction because the lattice has unitary spacing

$$v_2 = \begin{cases} \lambda_2 & \text{if particles in state 2 move rightward} \\ -\lambda_2 & \text{if particles in state 2 move leftward} \end{cases} \tag{81}$$

The two numbers α, β will vary in $[0, 1]$ since they represent the densities of the boundary reservoirs and for how we defined the injection and extraction rates they cannot exceed 1. The tumble rate has the two limiting cases of 0, where tumbling does not happen, and $+\infty$ where particles become random walkers, choosing randomly their direction at each step, but this loss of the persistent motion can be considered to be accomplished already with $\eta = 1$.
We will not consider values of η that are too small, because otherwise finite size effects become relevant in the model, with parts of the system that stay jammed for very long times. The importance of finite size effects in such a case has been discussed in [Kei+24], for the pausing TASEP which is analogous to $\lambda_2 = 0$ in our discussion, with the difference that the rates of processes $1 \to 2$ and $2 \to 1$ can be different.
Using the Gillespie algorithm it was possible to obtain data on the behavior of the system with open boundaries in the restricted parameter space we just described $\{\alpha \in [0,1], \beta \in [0,1], \eta \in (0,1], \lambda_2 \in [0,1), v_2/\lambda_2 \in \{-1,1\}\}$, but also to do simulations of the system with periodic boundary conditions in order to know the form of $J(\rho)$ and estimate the value of the maximum current reachable for given values of v_2 and η. Always keeping in mind the simple TASEP, results will be presented in a way that outlines several phase diagrams in the α-β plane, since the goal is to address how that phase diagram varies with v_2 starting from the one of the TASEP. For this reason we will use the same notation of the TASEP to classify the phases:

- LD stands for the input-controlled phase and J plotted against ρ_{bulk} reproduces the ascending branch of the fundamental diagram;

- HD stands for the output-controlled phase, $J(\rho_{\text{bulk}})$ reproduces the descending branch of the fundamental diagram;
- MC stands for the bulk-controlled phase, the current becomes independent of the boundary rates, and it takes the extremal value of the fundamental diagram.

In the following we investigate in detail some subcases, featuring some of the relevant behaviors of the system.

3.2.1 One direction of motion ($0 \leq v_2 < 1$)

The qualitative behavior of the system when all particles move rightward is similar to the simple TASEP and in fact all the three phases can be recognized pretty easily. In figure 14 it is possible

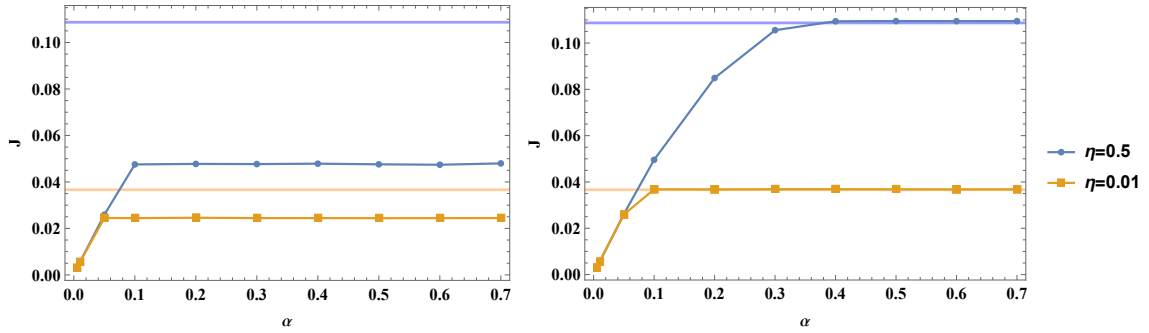

(a) $\beta = 0.1$ (b) $\beta = 0.8$

Figure 14: J as a function of α for $v_2 = 0.1$. Simulations for systems with $L = 500$. Symbols: OBCs. Horizontal lines: maximum current estimates, PBCs.

to see the phase transitions that can occur as α varies for two fixed values of β, the first one low enough to observe the phase transition from LD to HD figure 14a, and the second one high enough to get the phase transition from LD to MC figure 14b.
When λ_2 and η vary in the interval $[0, 1]$, the macroscopic effect on the system is a change in the phase diagram, where an enlargement of the area occupied by the MC phase can be observed. This is due to the decrease of the critical values α_c and β_c that mark the transitions from LD to MC and HD to MC respectively. These values seem to decrease by slowing down the species 2 particles and also by reducing the tumbling frequency. This means that the limiting effect on the flow of particles that is allowed in the bulk is becoming more prominent. This direct consequence of the presence of slow particles and the mechanisms through which they appear in the system should be better understood by doing some comparisons between the observed behavior of the model and the known behavior of the TASEP, as it has been attempted in the continuation of the section.
The first effect of having slow particles in the system is to reduce the maximum current reachable in the system, by limiting the mobility of all particles that fall behind a slow moving one. Considering the fundamental diagrams in figure 15, it is possible to observe that this effect becomes more severe as the tumble rate decreases. This can only be explained by the emergence of cooperative effects in the motion of particles that appear, due to the exclusion interaction. Consider the average trajectory of a single particle moving in an empty lattice, that is subject to the tumble dynamics: the average time spent in each state would be half the total time T taken to cross a lattice of length L. Knowing the average speed in each state, one lattice site per unit time in state 1 and λ_2 sites per unit time in state 2, one can evaluate the total time needed to cross the lattice and find that it is independent of the rate of tumble:

$$L = 1\frac{T}{2} + \lambda_2\frac{T}{2} \qquad \rightarrow \qquad T = \frac{2L}{1+\lambda_2} \tag{82}$$

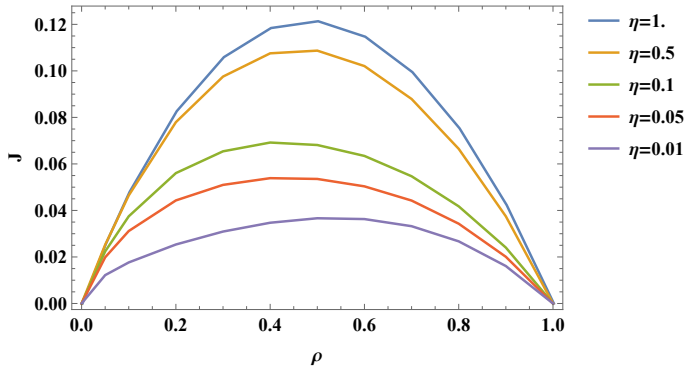

Figure 15: $J(\rho)$ for $\lambda_2 = 0.1$ and different η values. Simulations of the system with OBCs, with L=500

So the tumbling mechanism does not change the particles' average speed by itself. What is happening is that, when a particle slows down by going into state 2, it affects the particles behind it, creating a jam. The size of the resulting queues, which is the number of particles affected by a slow one ahead, is larger if the time spent in state 2 increases and this is what happens when η decreases. In the limit of $\eta \to 0$ the particles in state 2 are only the one that entered the lattice in that state and the system can be effectively described in terms of particles moving with rate λ_2 that have a finite extension [Bot17]. For higher values of the tumble rate this description cannot be successful because slow particles can appear inside a queue or disappear from its head, making the picture much more complex.

Another phenomenon that can be observed is the discrepancy between the occupations of the

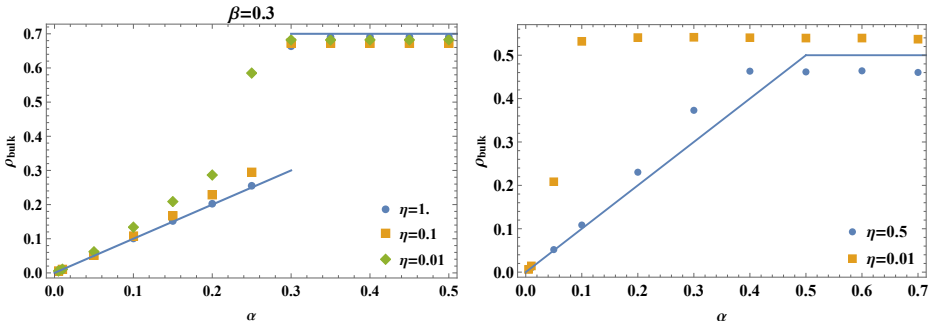

(a) $\beta = 0.3$ (LD to HD transition) (b) $\beta = 0.8$(LD to MC transition)

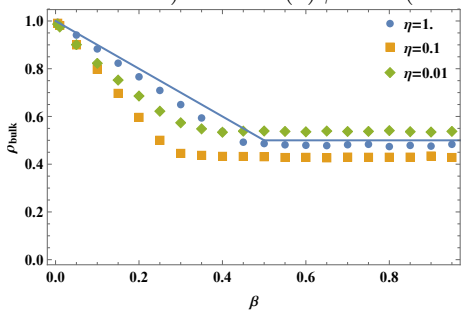

(c) ρ_{bulk} as a function of β for $\alpha = 0.8$, $\lambda_2 = 0.1$. Symbols: OBCs. Solid line: TASEP values of ρ_{bulk}, included for reference

Figure 16: ρ_{bulk} as a function of α for $\lambda = 0.1$. Simulations for systems with $L = 500$. Symbols: OBCs. Solid lines: TASEP predictions of ρ_{bulk}, included for reference

reservoir and the bulk densities. In phases other than MC, far enough from the boundaries the

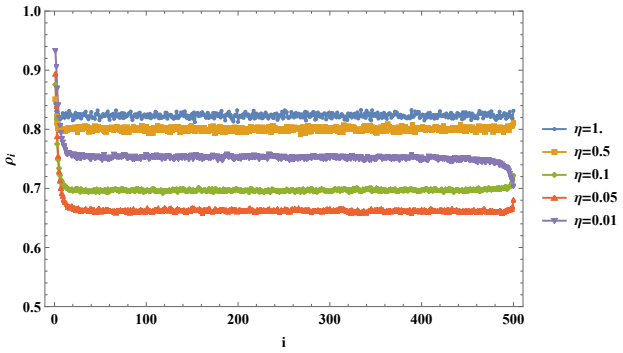

Figure 17: Density profiles $\{\rho_i\}_{i=1}^{L}$ for some η, with $\alpha = 0.8$, $\beta = 0.15$, $\lambda = 0.1$. Simulations for systems with $L = 500$.

density profile becomes flat, taking the value ρ_{bulk}, independent of the lattice site i. In the simple TASEP, ρ_{bulk} takes the value corresponding to the reservoir that is limiting the flow of particles, so in the LD phase $\rho_{\text{bulk}} = \rho_0 = \alpha$ and in the HD phase $\rho_{\text{bulk}} = \rho_{L+1} = 1 - \beta$. Conversely, in the presence of two species and with a finite tumbling rate, $\rho_{\text{bulk}} > \alpha$ is observed in the LD phase and $\rho_{\text{bulk}} < 1 - \beta$ in the HD phase. Since the density in the bulk is constant, we have that the current of the system must satisfy $J = J(\rho_{\text{bulk}})$[5] and so saying that J reaches its limiting value in the MC, implies that ρ_{bulk} approaches $\rho^* = \arg\max_{\rho\in[0,1]} J(\rho)$ as the system approaches the MC phase. For what we said before, the system reaches the condition $\rho_{\text{bulk}} = \rho^*$ before α and $1 - \beta$ reach that density value. If this were not true the critical values of the boundary rates could have increased with a smaller η instead of being always decreasing.
The discrepancy is affected by the value of η and tends to disappear as $\lambda_2 \to 1$, where the system becomes the simple TASEP. Plots where the phenomenon can be appreciated are displayed in figure16 and figure 16c, where we report a comparison of the values of ρ_{bulk} and the reservoir densities, obtained at fixed λ_2 and varying η, the simple TASEP results for ρ_{bulk} have also been included as reference.
Another observation is that the simulated density profiles show boundary layers that were not present in the simple TASEP. The new boundary layers can appear at the left (resp. right) end of the lattice in the LD phase (resp. HD phase), while ρ_{bulk} remains independent of β (resp. α). This means that at the boundaries there are some accelerations and decelerations of the particles, since motion in the bulk is affected by cooperative structures that correlate particles, while injection and extraction at the boundaries depend just on the first and last site, respectively, so that structures and correlations are neglected in some sense.

In the LD phase, with all the other parameters fixed, it seems that as η decreases, ρ_{bulk} always increases. From figure 16b it can be seen that the lower the value of η, the faster ρ_{bulk} grows with α so the maximum current phase is reached for smaller and smaller injection rates. The fact that ρ_{bulk} is lower than 0.5 for $\eta = 0.5$ and bigger for $\eta = 0.01$ should depend on the fact that the value of ρ that maximizes J has the same behavior, as can be seen in figure 15.
It must be specified that, due to BL the bulk density in the simulations is calculated by summing the stationary densities of the sites far enough from the boundaries, for example $\sum_{i=100}^{900} \rho_i$ on a lattice of size $L = 1000$. Furthermore in the MC phase, the density is not constant in the bulk so ρ_{bulk} plotted in the figure represents an average over sites.
The behavior of the HD phase seems less trivial: the density in the bulk remains consistently below the reservoir density $1-\beta$ but, instead of always decreasing, it can happen that ρ_{bulk} starts increasing for values of η low enough. This can be seen in figure 16b where some data for $\lambda = 0.1$ are reported.

3.2.2 Motion in both directions with a preferred one ($-1 < v_2 < 0$)

Now particles in state 2 move leftward and the behavior of the right reservoir changes. Also in this case the three phases can be found. In fact looking at the currents plotted against α, in figure18

[5] at least to a good approximation because the simulations cannot be done on an infinite system

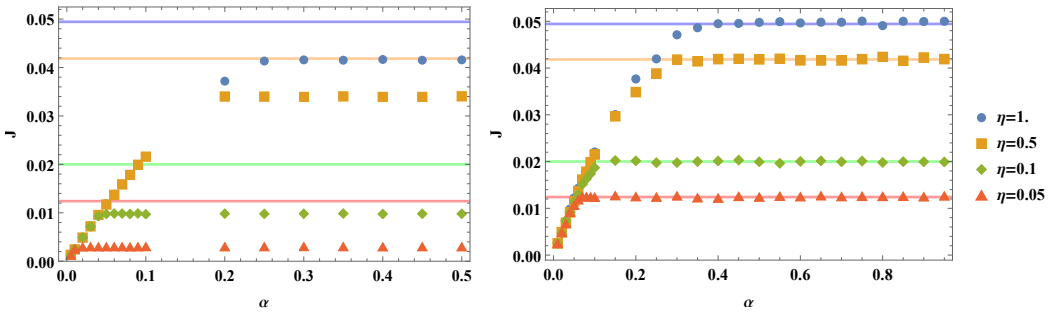

(a) $\beta = 0.3$, phase transition from LD to HD. (b) $\beta = 0.9$, phase transition from LD to MC.

Figure 18: Case $\lambda_2 = 0.5$. Simulations results for the current J, plotted against α for two values of β. Different values of η are considered, while the lattice size is $L = 500$. The horizontal lines are estimated values of maximum currents obtained from simulations of the PBCs system, they are needed as reference to distinguish between the HD and MC phases because in both cases the current becomes independent of the entry rate α.

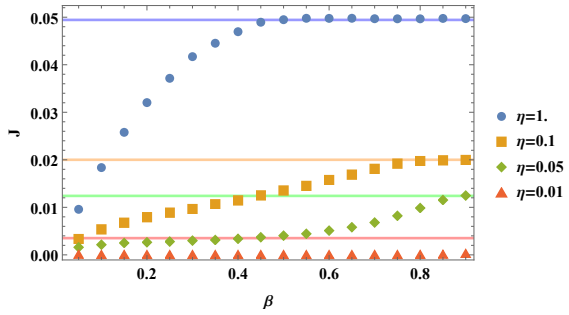

Figure 19: Case $\lambda_2 = 0.5$. Simulations results for the current J, plotted against β for $\alpha = 0.8$. Different values of η are considered. The horizontal lines are estimated values of maximum currents needed to distinguish between the LD and MC phases.

and figure19, the transitions between LD, HD and MC can be identified. The main difference in the phase diagram is, roughly speaking, that now the phase that tends to occupy the area of the diagram more than the others, is the HD phase, with the critical values of α and β respectively reducing and increasing when $\eta \to 0$ and $\lambda_2 \to -1$. Because of this fact it may become difficult to identify the MC and LD phases.

As in the previous case the system is affected by the collective behaviors of particles, with a difference: when $v_2 > 0$, particles in state 2 can create queues behind them, and in such structures the particles get slowed down but still move rightward. Now, a particle in state 2, at the right end of a sequence of occupied sites, prevents the others from moving, or, in other words, the particle clusters have fixed positions now. We stress that the latter thing is true also for $v_2 = 0$, but the fact that in this case particles do not move leftward makes it possible to have single particles that are stopped and so non-moving clusters can be composed of one particle, and this implies that $P_i[0, 2]$ is much higher with respect to the $v_2 < 0$ case, as it can be seen for $\eta = 0.1$ in figure 20.

Before discussing further the currents and the behavior of the OBCs system, let us take a small detour and discuss the formation of clusters in this case. Considering small values of η, the coalescence fragmentation picture used to obtain the average cluster size (see the final part of section 2.1) can be adapted to the case $v_2 \leq 0$:

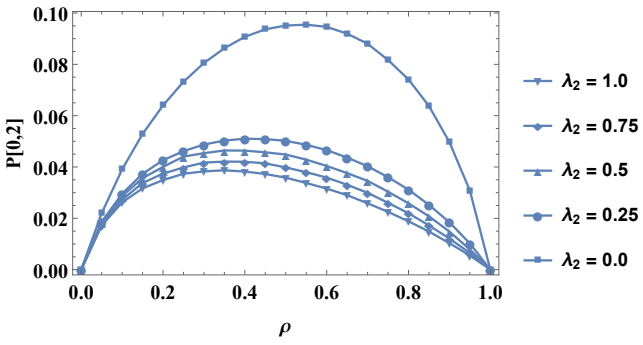

Figure 20: Case $v_2 \leq 0$. Plot of $P[0,2]$ as it varies with ρ in the PBCs system, with tumble rate $\eta = 0.1$. Symbols are the result of simulations done for a lattice $L = 500$

- when the leftward hopping rate is much bigger than the tumble rate $\lambda_2 \gg \eta$, the coalescence and fragmentation picture is totally analogous to the one discussed with the only difference that the rightward mass transfer is slower. When moving rightward a mass m^* takes roughly a time $m^*\,\lambda_2^{-1}$, as the motion of a single mass unit happens with rate λ_2. So (36) has to be modified for fragmentations triggered by the flip of a negative spin and one obtain a total rate of fragmentation equal to

$$r_f \simeq \sum_{k\geq 1} \eta\, n_c\, 2^{-k}\, \eta\, k\, \left(m^* + \frac{m^*}{\lambda_2}\right) = 2\left(1+\frac{1}{\lambda_2}\right)\eta^2\, n_c\, m^* \tag{83}$$

  which gives an average cluster size

$$l_c = \sqrt{\frac{2}{1+\lambda_2^{-1}}\frac{\rho}{(1-\rho)\eta}} \quad ; \tag{84}$$

- For $\lambda_2 = 0$ the description becomes different, masses cannot move rightward so a positive spin stops the masses. The consequence of this is that a mass can have a positive spin on its right side and remain still and mass transfers can only go leftward. The calculation of the total rate of coalescence has to be modified accordingly, because the distance between the original and the target site can be 1, and there is an additional spin that has to point in a given direction to allow the coalescence, so the rate becomes

$$r_c = \eta \sum_{n\geq 1} 2^{-n+1}\, n_c^2(1+\epsilon(n)) = 2\eta\, n_c^2 + O(\eta\, n_c^3) \tag{85}$$

  Also fragmentation changes a bit because the leftward mass transfers can be interrupted by all the k spins in between the original and the target site, while the flip of the right spin has no effect on the mass transfer. The calculation of r_f is the same given in equation (37) without the factor 2 because now only spin flips on the left of an occupied site can trigger a mass transfer

$$r_f \simeq \sum_{k\geq 1} \eta\, n_c\, 2^{-k}\, \eta\, k\, m^* = 2\,\eta^2\, n_c\, m^* \tag{86}$$

  So incidentally the two rates have changed by the same multiplicative factor and the average cluster size is the same as that of the PEP, namely

$$l_c = \sqrt{\frac{\rho}{(1-\rho)\eta}} \quad . \tag{87}$$

The comparison of these results with simulations can be found in figure 21, a good agreement can be observed. It is interesting that the pTASEP and the PEP produce the same cluster sizes, because

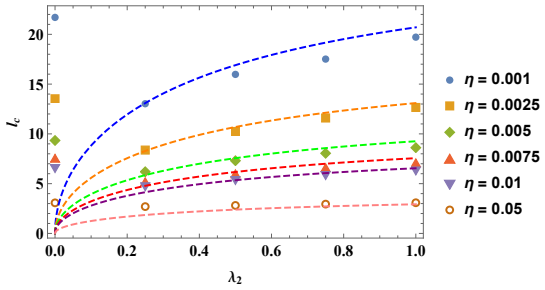

(a) Leftward hopping rate on the x-axis. Symbols: simulations. Dashed lines: coalescence fragmentation model prediction (see equation (84))

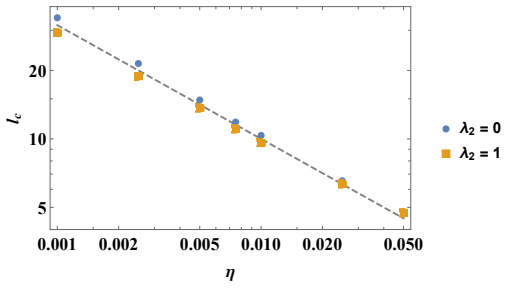

(b) Tumbling rate on the x-axis. Log-log scale. Symbols: simulations. Dashed line: coalescence fragmentation model prediction (see equation (87))

Figure 21: Average cluster size l_c obtained in simulations of the PEP with particles hopping leftward ($v_2 \leq 0$) with rate λ_2 and PBCs. Simulations done with $L = 1000$

this is true also in the uncorrelated limit $\eta \to \infty$. The data we collected showed that the whole distributions of the cluster sizes coincide, meaning that the two models share further connections between their statonary states even if the pTASEP sustains a current and the PEP does not. When $\lambda_2 \sim \eta$ the description we used does not hold because mass transfers happen too slowly rightward, so fragmentations in this direction happen easily but masses end up close to one another and spin flips can easily make them coalesce, making the assumption for the independent occupation of mass sites not applicable. The latter fact makes l_c deviate from (84), smoothly reaching its value at $\lambda_2 = 0$.

Now we go back to discussing the transport in the system. The current J in the system is smaller with respect to the case of particles moving in the same direction. The decrease of J_1 is less important than the negative contribution of J_2 (that now contains $P_i[0, 2]$ in place of $P_i[2, 0]$). In fact in figure 22a, it can be seen that J_1 does not change much when λ_2 varies from 0 to -1. Instead figure 22b shows how the fundamental diagrams changes with the tumble frequency η, for a given value of λ_2. The magnitude of the currents changes for other values of λ_2 but the effect of η is similar.

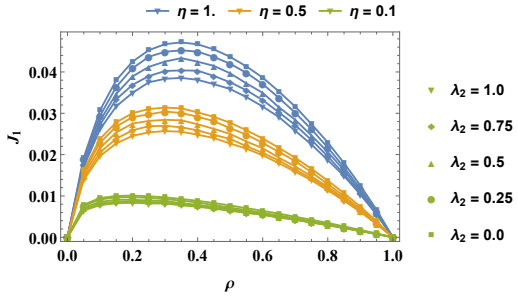

(a) Plot of $J_1(\rho)$ for different values of λ_2 and tumbling rate η.

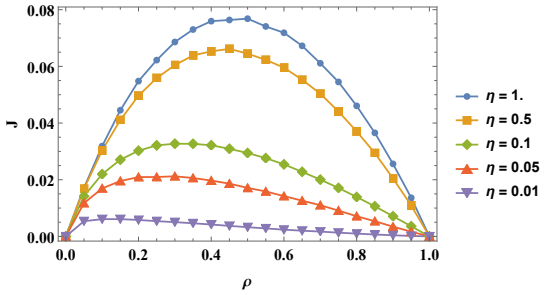

(b) Plot of the fundamental diagram $J(\rho)$ for $\lambda_2 = 0.25$ and different tumbling rates η.

Figure 22: Currents of leftward moving particles J_1 and total current J as a function of the particle density ρ, for the PEP with particles hopping leftward ($v_2 \leq 0$) with rate λ_2 and PBCs. Symbols are the result of simulations on systems of size $L = 500$

The fact that the HD phase becomes so important in the phase diagram, is due to the substantial change in the role of the right boundary condition. It changes from the role of a pure sink to being both a sink and a source of particles. In the previous case, the right reservoir could limit the flow of particles by reducing the amount of particles that are able to exit the system, now it has the

possibility of blocking the flow with the injection of a leftward moving particle. This blockage is more severe the smaller η is, because a particle in state 2 will tumble after a time $\frac{1}{\eta}$ on average. During the time in which no particle reaches the right reservoir, particles in state 2 can still be injected, filling the right part of the lattice even more. So we have that it becomes easier for the right reservoir to limit the flow in the system.
It can be argued that the filling of the system happens because the "equilibrium" of fragmentations and coalescence of gaps is broken in some way when the injection of particles at the right end of the system becomes too frequent.
As in the previous case, the density profile becomes flat far from the boundaries, so that a bulk density ρ_{bulk} can be defined.
The phenomenon of the additional boundary layers is present, similarly to the previous case, with the difference that now $\rho_{\text{bulk}} > 1 - \beta$ in the HD phase. When β is close to 0, the BL that forms at the left end of the lattice becomes increasing. This fact is consistent with the higher critical β marking the transition between HD and MC phase: when β varies from 0 to 1, ρ_{bulk} decreases, approaching the value ρ_* that maximizes the current, if the BL makes $\rho_{\text{bulk}} < 1 - \beta$ the critical β will be reached before with respect to the case of $\rho_{\text{bulk}} > 1 - \beta$.
The tumbling frequency plays a non-trivial role in making ρ_{bulk} exceed $1 - \beta$, because density variations at the BL become bigger as η decreases. This can be seen in figure 23a where ρ_{bulk} is plotted against β for different values of η, picking any value of β for which the system is in the HD phase; a decrease of the tumble frequency increases the bulk density.
Another phenomenon can be seen in the same figure, when η is low ($\lesssim 0.01$), it appears that ρ_{bulk} becomes independent of β in the HD phase, in most of the $[0, 1]$ interval. In figure 23b the plot of ρ_{bulk} is given for different values of λ_2, with $\eta = 0.01$ and more values of β considered to see what happens at its extremal values. From the figure it can be seen that if particles move quickly enough toward the left then the system always has the same behavior: the system almost fills up completely, with the gaps between particle clusters that prevent the bulk density from reaching 1, so below a certain threshold value of β the system saturates to a certain value of ρ_{bulk} which can be overcome only when the right reservoir density $1 - \beta$ exceeds the bulk density.

In figure 24 it can be seen that when the system saturates with clusters the current vanishes and that a condition of maximal current is always achieved which makes us say that, excluding $\lambda_2 = 1$ where $J(\rho) = 0$, the MC phase is always present (for $\lambda_2 = 0.95$ the estimate of the maximum current was poor, this because the system is close to the condition of symmetric hopping where the current in the translationally invariant system is 0).

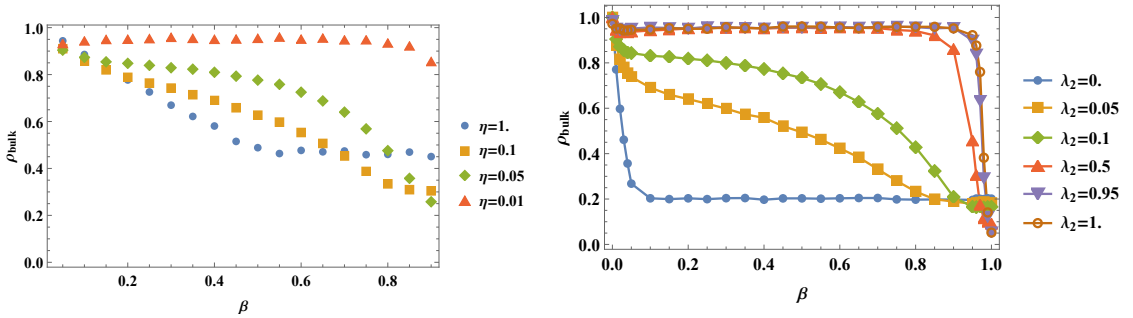

(a) Leftward jumping rate fixed $\lambda_2 = 0.5$

(b) Tumbling rate fixed $\eta = 0.01$

Figure 23: Data of the simulated ρ_{bulk}: points are taken for various extraction rates β. Lattice size $L = 1000$. The values of the left reservoir density is $\alpha = 0.8$ so the system is either in the HD or MC phase.

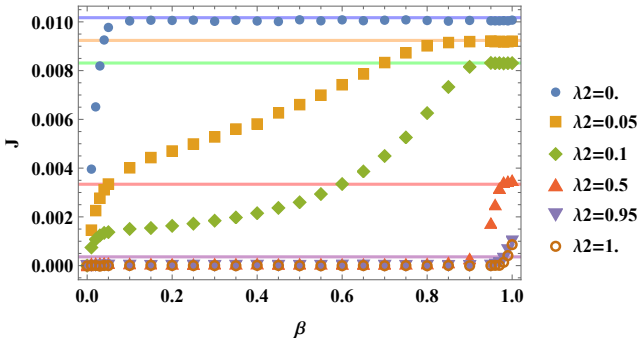

Figure 24: Current J as it varies with β, at fixed tumble rate $\eta = 0.01$ and for different values of the leftward hopping rate λ_2.

3.2.3 No preferred direction of motion ($v_2 = -1$)

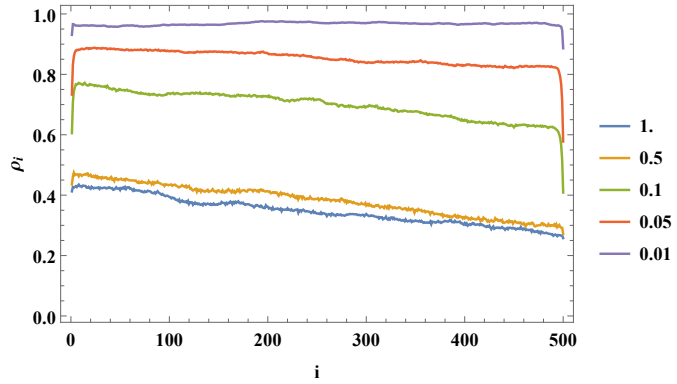

Figure 25: Simulated density profile, reported as they vary with η, while the rates of injection and extraction are $\alpha = 0.4$, $\beta = 0.75$. Lines are estimates of the maximal current of the phase diagram $J(\rho)$

Now particles move symmetrically, without directional bias. This means that the two reservoir play the same role and that transport between them has become purely diffusive, since the net contribution, due to different hopping rates amplitudes that make transport driven, has vanished. Without considering the persistent motion, this situation resembles that of the Symmetric Simple Exclusion Process(SSEP) with open boundary conditions [Sch01], a model analogous to the TASEP, where particles can hop to the right or the left. The solution of the SSEP, shows that at stationarity it gets established a density profile that interpolates linearly between the reservoir densities

$$\rho_i = \rho_0 - (\rho_0 - \rho_{L+1})\frac{i}{L} = \frac{\alpha(L-i) + (1-\beta)i}{L} \tag{88}$$

with the uniform current that satisfies Fick's law:

$$J_{\text{diff}} = \frac{\rho_0 - \rho_{L+1}}{L} = \frac{\alpha - (1-\beta)}{L} \tag{89}$$

A similar thing happens for the model we are considering: when $\eta \gtrsim 1$ the density profiles becomes almost linear, with the current that is proportional to the density

$$J = D\frac{\rho_0 - \rho_{L+1}}{L} \tag{90}$$

where D is the diffusion constant that deviates from 1 the rate of tumble is comparable with hopping rate $\eta \sim 1$. The fact that the density profile becomes linear can be seen in figure 25 where it can be seen how the density profile varies with η at fixed boundary rates. While the fact that the current is diffusive can be seen in figure 26 where the simulated J of the PEP with OBCs was plotted against

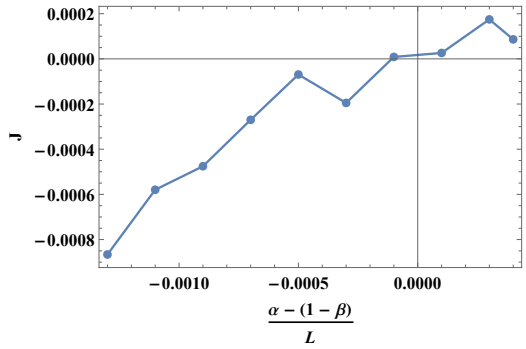

Figure 26: Dots represent the simulated current J in the PEP with OBCs plotted against the theoretical diffusive current (see equation (89)). Values are taken for α that varies with regular intervals from 0.1 to 0.9, while $\beta = 0.25$ and L=500.

J_{diff}. This result was also confirmed in [DCR20] where D was calculated by extending the MF mass model to systems with small density gradients.

When η decreases the system starts filling up with particles: unless the reservoir densities are close to 0, the system seems unable to sustain a non-vanishing current because the lattice is full of clusters that prevent the diffusion of particles. In figure 25 it can be seen how the density profile changes as η decreases, while in figure 27 it can be clearly seen that the current can become $\ll J_{\text{diff}}$ for most values of the injection rate α. The stationary current appears noisy in the simulations performed as it is linked to the vanishing density gradients between adjacent sites that make J_+ and J_- slightly different.

For $\eta = 0.01$, when α is close enough to 0, a current appears, this corresponds to the system

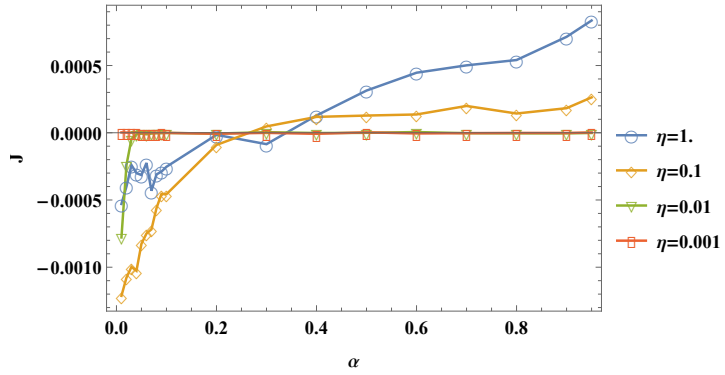

Figure 27: Dots represent the simulated current J in the PEP with OBCs plotted against α for $\beta = 0.75$ and L=500. More points were sampled near $\alpha = 0$.

becoming more empty, as it can be seen in figure 28, where the density per site saturates to an almost uniform profile for $\alpha > 0.05$, otherwise the particles concentrate in the right part of the lattice, where the reservoir density is higher, $\rho_{L+1} = 1 - \beta = 0.25$ in this case. To see how the

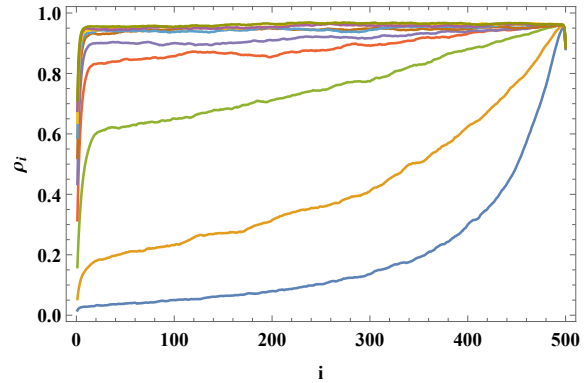

Figure 28: Simulated density profiles $\{\rho_i\}_{i=1}^{L}$ of the PEP with OBCs. With fixed parameters $\beta = 0.75$, $\eta = 0.01$, while α varies from 0.01 to 0.1 (from top to bottom) at regular intervals of 0.01.

system reaches the situation where the density can saturate we show plots of the mean density of the lattice evaluated as the total stationary density over the lattice size:

$$\frac{N}{L} = \frac{1}{L}\sum_{i=1}^{L} \rho_i \tag{91}$$

In figure 29, the latter quantity is plotted against the density of the left reservoir α, for various η while two values of β are considered. Comparing the two figures it can be seen that for $\eta \leq 0.01$ the occupation of the lattice does not change in a perceivable way for the two values of β considered. We imagine that there is an entire region of the α-β plane where the bulk density ρ_{bulk} becomes independent of the boundary conditions. The size of the region increases with η.

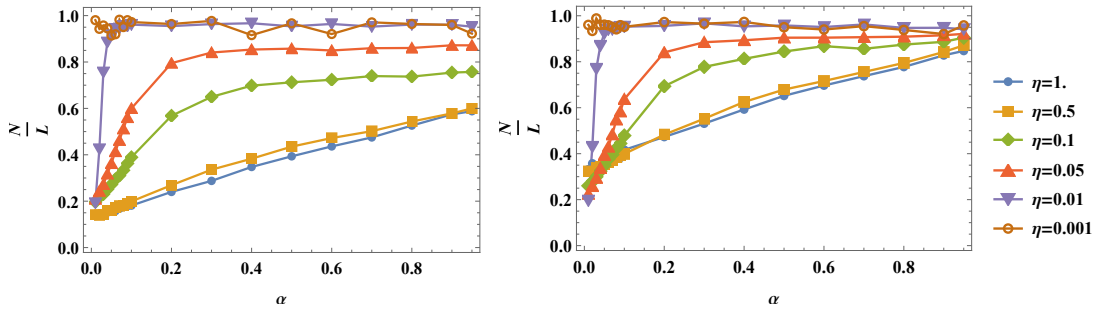

(a) $\beta = 0.75$ (b) $\beta = 0.25$

Figure 29: Mean density of the lattice defined in equation (91) as a function of the left reservoir density α, for various η. Simulations done for lattice of size $L = 500$.

4 Conclusions

In this study, we examined the persistent exclusion process following two routes. Initially, we evaluated how approximate methods are effective in characterizing the steady state of systems with periodic boundary conditions. Subsequently, we used simulations to investigate system behaviors when open boundaries and different particle velocities are included, leading us to a generalized model that allowed us to explore the phenomenology of OBCs in a wider framework that includes the well known TASEP as a special case.

The study of the PEP using the mass model and the pair approximation has presented the possibility to compare the effectiveness of the particle oriented MF against MF cluster approximation which is instead site oriented, which had not been done previously in the literature. Comparing the two MF methods has showed that the gap oriented method represents always an improvement with respect to the PA: as one could have expected the MF mass model is much better in describing the gap distributions as this is the core of the approximation, at the same time both methods neglect particle correlations beyond nearest-neighbor pairs but the quantitative predictions of these are improved by accounting correlations between vacant sites. The we have introduced the Generalized Persistent Exclusion Process which offers a versatile framework for probing biological and synthetic systems, from bacterial colonies to intracellular transport, even if the model as a whole cannot be traced to a biological system. The phenomenology of the generalized model has proven to be very rich, regardless of the direction of motion of the particles of species 2, collective phenomena become dominating in the model with the particles that form larger and larger structures as the rate with which particles change state decreases. The results presented in section 3.2.2 regarding the coalescence-fragmentation model show how a reframing that focuses on gaps description can be useful in such contexts of emerging collective behaviors. Such variety has prevented us from using approximations on the generalized model in this thesis due to lack of time. It remains of interest to test at least the PA on the OBCs system we investigated. Some preliminary attempts not included

in this report have shown that the PA applied to the $v_2 < 0$ OBCs system seem to show some periodicity, with the system that empties and refills over time, something that resembles what has been described in [Kei+24]. The latter work studies the pausing TASEP, which corresponds to our model with $v_2 = 0$, to describe transcription bursts performed by ribosomes that can be inhibited and they discussed how this phenomenon is linked to finite size effects. It would be interesting to see how the PA performs in describing this behavior, and in general it could be profitable to focus further researches on specific phenomena that have emerged in our OBCs system. Important finite size effects are known to be present also in the PEP [CMT23].
Restricting the rates of injection and extraction to values that describe the coupling to reservoirs has allowed to facilitate the exploration of the phenomenology of the OBCs system, representing both a reduction of the space of parameters that needed to be considered and a tool for creating interpretations of what was happening.
Our system has proven to be able to undergo boundary induced phase transitions analogous the ones of the TASEP despite having counterflowing particles, as long as the fundamental diagram is different from $J(\rho) = 0$. Even in the latter case, which corresponds to the symmetric PEP, the system shows a non trivial behavior as we have unveiled the presence of a region of the α-β phase diagram where the system reaches a saturated state where the number of particles in the system becomes independent of the boundary conditions and the current vanishes. We have observed a trace of this regime also in the HD phase of the system with a preferred motion direction. This behavior seems to be novel in the field of driven lattice gases and it may be related with condensation transitions observed in mass transport model with open boundaries [LMS05]. We have not fully explored any route in the development of a theory that could explain it but we believe this could be done in further researches. Other inspirations for further research are the development of a theory that is able to predict the location of the transitions between LD, HD, MC phases and explain the observed boundary effects, very different from the well-known TASEP ones, that make the bulk density depend non-trivially on the occupation of the boundary reservoirs. It may be worth exploring generalizations of the domain wall theory like the one proposed in [MSR11].
A remarkable result has been the finding that the pTASEP and the PEP share the same statistics for their clusters sizes, so that the only qualitative difference between the two systems is that the first is able to sustain a current while the other is characterized by a zero net current at stationarity. It is interesting because it means that observing temporal snapshots of the configurations is not enough to distinguish one model from the other. The similarity of the cluster size distributions has been verified in simulations and a heuristic argument valid at low rate of tumble confirms the equality of their average, what we have done here does not exhaust the possibility to further explore the connection between the two systems. Our generalized model could be used to further explore these and the other effects we cited in a unified framework.

A Gillespie Algorithm

The Gillespie algorithm, is an efficient way of simulating continuous-time Markov processes [Gil76]. In short, the algorithm produces a new configuration starting from an initial one by evaluating first the time necessary for the transition to occur and then the new configuration, in this way the algorithm does not require any rejection steps, making the simulation of a trajectory 100% efficient.

A.1 Algorithm Overview

Consider a system in an initial configuration $\mathcal{C}$ at time t_0. Let $W_{\mathcal{C}\mathcal{C}'}$ represent the transition rate from the current configuration to a new configuration $\mathcal{C}'$. Let $\mathcal{S}$ be the set of all possible configurations in which $\mathcal{C}$ can do a transition. Knowing that the times of occurrence of each transition $\mathcal{C} \to \mathcal{C}_1$ obey exponential distributions with average time $\frac{1}{W_{\mathcal{C}\mathcal{C}_1}}$, the most straightforward way to simulate a trajectory would be to sample all these times and pick the smallest one τ, at least a fraction of the sampled times will be discarded, leading to the inefficiency Gillespie was able to eliminate.
The algorithm samples directly τ, which is a stochastic variable, that is the time elapsed from t_0 to

the transition to the new configuration, its probability distribution is equivalent to the probability that none of the available transitions has occurred in the infinitesimal time steps dt that compose τ:

$$P(\tau) = \lim_{\Delta t \to 0} \left(1 - \Delta t \sum_{\mathcal{C}' \in \mathcal{S}} W_{\mathcal{C}\mathcal{C}'}\right)^{\frac{\tau}{\Delta t}} = \exp\left(-\tau \sum_{\mathcal{C}' \in \mathcal{S}} W_{\mathcal{C}\mathcal{C}'}\right) \tag{92}$$

So the time of the next transition can be sampled from the latter distribution given the transition rates $W_{\mathcal{C}\mathcal{C}'}$. It can be shown that the probability that the process $\mathcal{C}\mathcal{C}_1$ has produced the smallest time τ is:

$$P(\mathcal{C} \to \mathcal{C}_1) = \frac{W_{\mathcal{C}\mathcal{C}_1}}{\sum_{\mathcal{C}' \in \mathcal{S}} W_{\mathcal{C}\mathcal{C}'}} \tag{93}$$

In order to implement this method it will be sufficient to generate two random numbers, uniformly distributed in the interval $[0, 1]$ ξ_1 and ξ_2 and to use them in the following equations where the possible transitions have numerated, so that rate labels $\mathcal{C}\mathcal{C}'$ get replaced by $l \in \{1, ..., K\}$, with $K = |\mathcal{S}|$, and becomes possible to write:

$$\tau = -\frac{1}{\sum_{l=1}^{K} W_l} \ln \xi_1, \tag{94}$$

$$\sum_{l=1}^{k-1} W_l < \xi_2 \sum_{l=1}^{K} W_l \leq \sum_{l=1}^{k} W_l \tag{95}$$

The Gillespie algorithm implemented for the models considered in this work does the following operations:

1. Set the values for the parameters, the initial configuration $\mathcal{C}_0$ and the maximum time the trajectory can reach T.
2. Having enumerated all processes that are possible in the model, it is now necessary to associate the rate, calculated from the parameters, to the processes that can actually occur in the system in configuration $\mathcal{C}_0$, all the other processes will have rate 0, so that when the configuration changes it will be sufficient to update the collection of rates without enumerating them every time.
3. Generate a random number ξ_1 and use equation (94) to compute τ. Update the total elapsed time to $t' = t + \tau$.
4. Generate a second random number ξ_2 and choose the next transition k by checking which inequality in equation (95) is satisfied. Based on the result, identify the specific transition.
5. Update the state of the system and the rates with the new processes available and set to 0 the ones that are not possible anymore (this is convenient in the model considered here because when something happens on a lattice site it affects at most its next-nearest neighbors)
6. Repeat steps 3–5 until the elapsed time is smaller then T.

This is the basic algorithm, then in order to collect data on the trajectory, configurations $\mathcal{C}$ were sampled at time intervals larger than a given value Δt. A quantity of interest can then be evaluated by averaging over the sampled configurations. For example the density of particles in one state:

$$\rho_{s,i} = \frac{1}{\#\text{ of samples}} \sum_{\mathcal{C} \in \text{samples}} \mathbb{1}\left[n_i^{\mathcal{C}} = s\right] \tag{96}$$

The other average quantities were obtained in similar ways. To have an appropriate Δt, it has been usually chosen to use a value proportional to the inverse rate of the slowest process present in the system[6].

[6]Most of the time this has been the tumble of a particle, so $\Delta t = \eta^{-1}$

Bibliography

[bK92] D. ben-Avraham and J. Köhler. "Mean-field (n, m)-cluster approximation for lattice models". In: *Physical Review A* 45.12 (June 1992), pp. 8358–8370. ISSN: 1094-1622. DOI: 10.1103/physreva.45.8358. URL: http://dx.doi.org/10.1103/PhysRevA.45.8358.

[Ber04] H.C. Berg. *E. coli in Motion*. Biological and Medical Physics, Biomedical Engineering. Springer, 2004. ISBN: 9780387008882. URL: https://books.google.it/books?id=qyVoI1iUiBkC.

[Bot17] Alessandro Giacomo Bottero. "Analysis of a two species TASEP as a model for heterogeneous transport on microtubules". MA thesis. Ludwig Maximilian University of Munich, 2017.

[Cat12] M E Cates. "Diffusive transport without detailed balance in motile bacteria: does microbiology need statistical physics?" In: *Reports on Progress in Physics* 75.4 (Mar. 2012), p. 042601. ISSN: 1361-6633. DOI: 10.1088/0034-4885/75/4/042601. URL: http://dx.doi.org/10.1088/0034-4885/75/4/042601.

[CT15] Michael E. Cates and Julien Tailleur. "Motility-Induced Phase Separation". In: *Annual Review of Condensed Matter Physics* 6.1 (Mar. 2015), pp. 219–244. ISSN: 1947-5462. DOI: 10.1146/annurev-conmatphys-031214-014710. URL: http://dx.doi.org/10.1146/annurev-conmatphys-031214-014710.

[CMT23] Jim Chacko, Sudipto Muhuri, and Goutam Tripathy. "Clustering and finite size effects in a two-species exclusion process". In: *Indian Journal of Physics* 98.4 (Sept. 2023), pp. 1553–1560. ISSN: 0974-9845. DOI: 10.1007/s12648-023-02880-z. URL: http://dx.doi.org/10.1007/s12648-023-02880-z.

[CMZ11] T Chou, K Mallick, and R K P Zia. "Non-equilibrium statistical mechanics: from a paradigmatic model to biological transport". In: *Reports on Progress in Physics* 74.11 (Oct. 2011), p. 116601. ISSN: 1361-6633. DOI: 10.1088/0034-4885/74/11/116601. URL: http://dx.doi.org/10.1088/0034-4885/74/11/116601.

[DCR20] Rahul Dandekar, Subhadip Chakraborti, and R. Rajesh. "Hard core run and tumble particles on a one-dimensional lattice". In: *Physical Review E* 102.6 (Dec. 2020). ISSN: 2470-0053. DOI: 10.1103/physreve.102.062111. URL: http://dx.doi.org/10.1103/PhysRevE.102.062111.

[Der+93] B Derrida et al. "Exact solution of a 1D asymmetric exclusion model using a matrix formulation". In: *Journal of Physics A: Mathematical and General* 26.7 (Apr. 1993), pp. 1493–1517. ISSN: 1361-6447. DOI: 10.1088/0305-4470/26/7/011. URL: http://dx.doi.org/10.1088/0305-4470/26/7/011.

[Dol+20] Pritha Dolai et al. "Universal scaling in active single-file dynamics". In: *Soft Matter* 16.30 (2020), pp. 7077–7087. ISSN: 1744-6848. DOI: 10.1039/d0sm00687d. URL: http://dx.doi.org/10.1039/d0sm00687d.

[EWG15] J Elgeti, R G Winkler, and G Gompper. "Physics of microswimmers—single particle motion and collective behavior: a review". In: *Reports on Progress in Physics* 78.5 (Apr. 2015), p. 056601. ISSN: 1361-6633. DOI: 10.1088/0034-4885/78/5/056601. URL: http://dx.doi.org/10.1088/0034-4885/78/5/056601.

[Gil76] Daniel T Gillespie. "A general method for numerically simulating the stochastic time evolution of coupled chemical reactions". In: *Journal of Computational Physics* 22.4 (Dec. 1976), pp. 403–434. ISSN: 0021-9991. DOI: 10.1016/0021-9991(76)90041-3. URL: http://dx.doi.org/10.1016/0021-9991(76)90041-3.

[Kei+24] Johannes Keisers et al. *Biologically relevant finite-size effects in a driven lattice gas with particle pausing and dynamical defects*. 2024. DOI: 10.48550/ARXIV.2406.16569. URL: https://arxiv.org/abs/2406.16569.

[KRB10] Pavel L. Krapivsky, Sidney Redner, and Eli Ben-Naim. *A Kinetic View of Statistical Physics*. Cambridge University Press, Nov. 2010. ISBN: 9780511780516. DOI: 10.1017/cbo9780511780516. URL: http://dx.doi.org/10.1017/CBO9780511780516.

[Kru91] Joachim Krug. "Boundary-induced phase transitions in driven diffusive systems". In: *Physical Review Letters* 67.14 (Sept. 1991), pp. 1882–1885. ISSN: 0031-9007. DOI: 10.1103/physrevlett.67.1882. URL: http://dx.doi.org/10.1103/PhysRevLett.67.1882.

[LMS05] E. Levine, D. Mukamel, and G. M. Schütz. "Zero-Range Process with Open Boundaries". In: *Journal of Statistical Physics* 120.5–6 (Sept. 2005), pp. 759–778. ISSN: 1572-9613. DOI: 10.1007/s10955-005-7000-7. URL: http://dx.doi.org/10.1007/s10955-005-7000-7.

[MGP68] Carolyn T. MacDonald, Julian H. Gibbs, and Allen C. Pipkin. "Kinetics of biopolymerization on nucleic acid templates". In: *Biopolymers* 6.1 (Jan. 1968), pp. 1–25. ISSN: 1097-0282. DOI: 10.1002/bip.1968.360060102. URL: http://dx.doi.org/10.1002/bip.1968.360060102.

[MSR11] Sudipto Muhuri, Lenin Shagolsem, and Madan Rao. "Bidirectional transport in a multispecies totally asymmetric exclusion-process model". In: *Physical Review E* 84.3 (Sept. 2011). ISSN: 1550-2376. DOI: 10.1103/physreve.84.031921. URL: http://dx.doi.org/10.1103/PhysRevE.84.031921.

[MRM23] Indranil Mukherjee, Adarsh Raghu, and Pradeep Kumar Mohanty. "Nonexistence of motility induced phase separation transition in one dimension". In: *SciPost Physics* 14.6 (June 2023). ISSN: 2542-4653. DOI: 10.21468/scipostphys.14.6.165. URL: http://dx.doi.org/10.21468/SciPostPhys.14.6.165.

[PG13] Itai Pinkoviezky and Nir S Gov. "Modelling interacting molecular motors with an internal degree of freedom". In: *New Journal of Physics* 15.2 (Feb. 2013), p. 025009. ISSN: 1367-2630. DOI: 10.1088/1367-2630/15/2/025009. URL: http://dx.doi.org/10.1088/1367-2630/15/2/025009.

[SCN11] Andreas Schadschneider, Debashish Chowdhury, and Katsuhiro Nishinari. "Stochastic Transport in Complex Systems: From Molecules to Vehicles". In: *Stochastic Transport in Complex Systems*. Elsevier, 2011. ISBN: 9780444528537. DOI: 10.1016/b978-0-444-52853-7.00016-6. URL: http://dx.doi.org/10.1016/B978-0-444-52853-7.00016-6.

[SS97] Andreas Schadschneider and Michael Schreckenberg. "Car-oriented mean-field theory for traffic flow models". In: *Journal of Physics A: Mathematical and General* 30.4 (Feb. 1997), pp. L69–L75. ISSN: 1361-6447. DOI: 10.1088/0305-4470/30/4/005. URL: http://dx.doi.org/10.1088/0305-4470/30/4/005.

[Sch01] G.M. Schütz. "Exactly Solvable Models for Many-Body Systems Far from Equilibrium". In: *Phase Transitions and Critical Phenomena*. Elsevier, 2001, pp. 143–144. DOI: 10.1016/s1062-7901(01)80015-x. URL: http://dx.doi.org/10.1016/S1062-7901(01)80015-X.

[SG14] Rodrigo Soto and Ramin Golestanian. "Run-and-tumble dynamics in a crowded environment: Persistent exclusion process for swimmers". In: *Physical Review E* 89.1 (Jan. 2014). ISSN: 1550-2376. DOI: 10.1103/physreve.89.012706. URL: http://dx.doi.org/10.1103/PhysRevE.89.012706.

[TC08] J. Tailleur and M. E. Cates. "Statistical Mechanics of Interacting Run-and-Tumble Bacteria". In: *Physical Review Letters* 100.21 (May 2008). ISSN: 1079-7114. DOI: 10.1103/physrevlett.100.218103. URL: http://dx.doi.org/10.1103/PhysRevLett.100.218103.

[Tho+11] A G Thompson et al. “Lattice models of nonequilibrium bacterial dynamics”. In: *Journal of Statistical Mechanics: Theory and Experiment* 2011.02 (Feb. 2011), P02029. ISSN: 1742-5468. DOI: 10.1088/1742-5468/2011/02/p02029. URL: http://dx.doi.org/10.1088/1742-5468/2011/02/P02029.